

Reuse of Flowback and Produced Water: The Effects of Treatment Process on Tight-Rock Wettability and Selective Removal of Problematic ions for Stability of Friction Reducers

By

Yanze Zhang

A thesis submitted in partial fulfillment of the requirements for the degree of

Master of Science

in

Petroleum Engineering

Department of Civil & Environmental Engineering
University of Alberta

© Yanze Zhang, 2022

Abstract

Oil and gas industry have faced significant operational, economic, and environmental challenges in recycling produced water. The treatment of produced water is highly researched, but few studies have evaluated the performance of treated produced water when used for hydraulic fracturing and enhanced oil recovery (EOR) operations.

In this study, we treated various aqueous solutions, including synthetic formation brine (FB), sodium chloride (NaCl), calcium chloride (CaCl₂), and sodium sulfate (Na₂SO₄), using an electro-oxidation (EO) process. The brine properties, including density, surface tension (ST), oil–water interfacial tension (IFT), viscosity, and pH, were compared before and after the treatment. Then, we conducted systematic contact-angle (CA) measurements and spontaneous imbibition tests using treated and untreated brine to study the effects of water treatment on rock–fluid interactions and its impact on oil recovery. The experimental results show that the effect of the EO process on ST, density, viscosity, and IFT was insignificant. However, the CA results show that the treated FB, NaCl, and Na₂SO₄ solutions exhibit stronger wetting characteristics compared with the untreated ones, while the treated CaCl₂ solution exhibit weaker wetting characteristics compared with the untreated ones. We hypothesized that the change in the wetting characteristics was due to the generated oxidants from the EO process. We added OH⁻, H⁺, hydrogen peroxide (H₂O₂), and sodium hypochlorite (NaOCl) into untreated brine to test this hypothesis and monitored the CA variations. The results suggest that H₂O₂ and OH⁻ can alter the wettability to more water-wet conditions in the NaCl solution but not in the CaCl₂ solution. Furthermore, NaOCl results in wettability alteration to more oil-wet conditions in NaCl and CaCl₂ solutions. The change in wettability to more water-wet conditions is mainly the result of the oxidation of dissolved organic

matters, and the change to more oil-wet conditions is the result of the dissolution of high-valence cations, causing the cation bridging effect.

We also studied the compatibility between produced formation brine and hydrolyzed polyacrylamide (HPAM). In our study, we conducted dynamic viscosity, particle size distribution, and viscoelasticity measurements to evaluate the performance of HPAM in DI water and formation brine (FB). The experimental results suggest that HPAM in FB has a much lower dynamic viscosity and shear stress profiles than in DI water. The storage modulus is higher than the loss modulus in the entire measured range when adding HPAM into FB, indicating a considerable curling of HPAM in the FB. We also conduct a sensitivity analysis to identify the problematic ions and their threshold concentration in the FB through dynamic viscosity measurement. Our results show that HPAM can only resist monovalent ions at low concentrations (<1,000 ppm). The presence of divalent ions and iron ions at low concentrations (<1,000 ppm, and <100 ppm, respectively) may cause HPAM molecules to curl and significantly lose dynamic viscosity. The iron ions concentration at 1,000 ppm can cause HPAM molecules permanent damage.

Preface

This thesis is an original work by Yanze Zhang.

Chapter 2, 3, 4, and 5 of this thesis has been published as Y Zhang, L Yuan, M Sadrzadeh, H Dehghanpour (2022). Effects of Electro-Oxidation Process on Tight-Rock Wettability and Imbibition Oil Recovery. Energy & Fuels. And Zhang, Y., Yuan, L., Jakhete, S., Sadrzadeh, M., & Dehghanpour, H. (2021, December). Application of Electro-oxidation Technology for Water Treatment and Rock Wettability Alteration. In Unconventional Resources Technology Conference, Unconventional Resources Technology Conference (URTeC).

Chapter 6, 7, and 8 are ongoing work, but will be published in SPE Hydraulic Fracturing Technology Conference and Exhibition 2023

I was responsible for conducting laboratory experiments, analyzing the experimental data as well as writing and editing these papers. Dr. Mohtada Sadrzadeh and Dr. Hassan Dehghanpour (supervisory author) and were responsible for reviewing the paper and providing technical feedbacks.

Dedication

To my dearest parents,

Mrs. Hongxia Wu, and Mr. Huisheng Zhang.

And my beloved grandparents

Acknowledgements

I would like to express my sincere gratitude to my supervisor Dr. Hassan Dehghanpour for his patient and insightful guidance, continuous support, kind encouragement throughout my master study. I would also like to express my gratitude and respect to Dr. Mohtada Sadrzadeh for giving many useful technical advises. Without their help, this thesis would not be complete.

I would also like to express my appreciation from my bottom of my heart to my parents Mr. Huisheng Zhang and Mrs. Hongxia Wu, and grandparents Mrs. Jufang Ye, Mrs. Youlan Wang, and Mr. Chunde Zhang (passed away in 2021) for their moral support, continuous understanding and encouragement.

I would like to give my special thanks to Lin Yuan for her valuable comments, suggestions, and assistance on my research. She gave me many guidance and help, especially at the beginning of my M.Sc. study.

I would like to thank my past and present colleagues (Mohammad Yousefi, Shiyu Xu, Maryam Eghbalvala, Mohammad Sabbir Hossain, Son Tran, Tamer Moussa, Amin Alinejad, Jestril Ebagalolo, Wajid Ali and Zhanyuan Liu) for their insightful contributions and valuable discussions.

I would also like to acknowledge the Natural Sciences and Engineering Research Council of Canada (NSERC) for providing the research funding for this study.

Tables of Contents

Abstract.....	ii
Preface.....	iv
Dedication	v
Acknowledgements	vi
Chapter 1 Introduction.....	1
1.1 Background	1
1.2 Preview of the Study	2
1.3 Objectives of Research.....	3
1.4 Structure of Thesis	3
Chapter 2 Literature Review of Water Treatment on Rock-fluid Interaction	5
2.1 Review of Water Treatment Methods	5
2.2 Electro-oxidation Water Treatment Method	5
2.3 Chemical Interactions between Oxidants and Rock.....	7
2.4 Research Gaps	8
Chapter 3 Effect of Electro-oxidation Process on Fluid Physical Properties.....	9
3.1 Materials.....	9
3.1.1 Fluid Samples.	9
3.2 Methodology	10
3.2.1 EO Treatment.	10
3.2.2 Surface Tension, Density, Viscosity, and Interfacial Tension Measurements.	10
3.3 Results and Discussion.....	12
3.3.1 Oxidants Generated by the EO Process.....	12
3.3.2 Effects of EO Treatment on the Physical Properties of Aqueous Solutions.	13
Chapter 4 Effect of Electro-oxidation Process on Tight-rock Wettability	17

4.1 Materials.....	17
4.1.1 Rock Samples.	17
4.1.2 Fluid Samples.	18
4.2 Methodology	19
4.2.1 CA Measurements.	19
4.3 Results	21
4.3.1 Equilibrated CA under Limiting Conditions.	21
4.3.2 Change in Oil CA upon the Addition of OH ⁻ , H ⁺ , and Oxidants.	23
4.4 Discussion	27
4.4.1 Effect of pH on CA Change.	27
4.4.2 Effect of Cation Bridging on CA.....	29
4.4.3 Effect of Oxidants on CA.	31
Chapter 5 Effect of Electro-oxidation on the spontaneous imbibition.....	35
5.1 Materials.....	35
5.1.1 Rock Samples.	35
5.1.2 Fluid Samples.	35
5.2 Methodology	35
5.2.1 Spontaneous Imbibition Tests.	35
5.3 Results and Discussion.....	36
5.3.1 Imbibition Oil Recovery Results.	36
5.3.2 Precipitation in Spontaneous Imbibition Tests.	38
Chapter 6 Literature Review on Fracturing Fluid and Research Gap.....	42
6.1 Review on Hydraulic fracturing and Friction Reducer	42
6.2 Research Gap.....	44
Chapter 7 Problems with Reuse of Untreated Brine for Hydraulic Fracturing.....	46

7.1 Material	46
7.1.1 Friction Reducer.	46
7.1.2 Fluid Sample.....	46
7.2 Methodology	46
7.2.1 Sample Preparation.....	46
7.2.2 Density and Surface Tension Measurements.....	47
7.2.3 Particle Size Distribution Measurements	47
7.2.3 Dynamic Viscosity and Viscoelasticity Measurement	48
7.3 Results and Discussion.....	48
7.3.1 Density and Surface Tension Measurement	48
7.3.3 Particle Size Distribution of HPAM.....	51
7.3.4 Viscoelastic Properties Measurements	53
Chapter 8 The Effect of Cations and its Salinity on Shear Viscosity	56
8.1 Material	56
8.1.1 Friction Reducer.	56
8.1.2 Fluid Samples.	56
8.2 Methodology	56
8.2.1 Sample Preparation.....	56
8.2.2 Dynamic Viscosity Measurements.	57
8.3 Results and Discussions	57
8.3.1 Density and Surface Tension Measurements.....	57
8.3.2 Shear Viscosity Measurements.....	58
8.3.3 Impact of Salinity on Dynamic Viscosity and Shear Stress	60
8.3.4 Impact of Cation Valence on Dynamic Viscosity and Shear Stress.....	61
8.3.5 Impact of Iron Ions on the Stability of the HPAM Solution	61

Chapter 9 Limitation, Future Work, and Conclusion.....	65
9.1 Limitation and Future Work.....	65
9.2 Conclusion.....	67
Chapter 10 Reference	71

List of Tables

Table 3.1 Original ion composition of brine..... 9

Table 3.2 Concentration difference of generated oxidants by EO process before and after treatment 13

Table 3.3 The measured ST, density, viscosity, and pH of brine before and after the EO process 14

Table 3.4 Summary of measured IFT between oil and treated/untreated brine..... 15

Table 3.5 The measured IFT values between oil and 90,000 ppm treated and untreated brine. .. 16

Table 4.1 Properties of the Montney core plugs used in this study. 18

Table 4.2 The mineralogy of the core plugs determined from XRD method. 18

Table 4.3 Concentration and volume of chemical additives added to the base aqueous solutions. 21

Table 4.4 The interaction and equilibrium constant at 25°C for oil-water and rock-water interfaces (Sanaei et al., 2019; Zeng et al., 2019). (- for the oil phase and > for rock surface) 30

Table 5.1 The produced oil and calculated oil recovery factor for each case..... 38

Table 5.2 Picture of rock samples used in the spontaneous imbibition tests using 90,000 ppm (a-d) untreated NaCl; (e) treated NaCl; (f) untreated NaCl + NaOCl; (g) untreated NaCl+ H₂O₂ (h) treated NaCl. 41

Table 7.1 Measured value of density and surface tension of HPAM solutions..... 49

Table 7.2 Power-law parameter, including power-law consistency factor (K) and flow behavior index (n), and R-squared value for HPAM solution..... 50

Table 7.3 The average hydrodynamic size of the HPAM and its standard deviation..... 52

Table 8.1 Measured value of density and surface tension of HPAM in different aqueous solutions 58

Table 8.2 Power-law parameter, including power-law consistency factor (K) and flow behavior index (n), and R-squared values for HPAM in different aqueous solutions..... 60

List of Figures

Figure 3.1 Spinning drop tensiometer.....	11
Figure 3.2 The instrument used for physical properties measurements: (a) SIGMA 700 Tensiometer and (b) Brookfield Viscometer	12
Figure 3.3 The concentration of (a) active chlorine and (b) H ₂ O ₂ after 3, 6, and 9 days of the EO process. Note that active chlorine and H ₂ O ₂ do not exist in untreated brine.	13
Figure 4.1 The instrument used for CA measurements	19
Figure 4.2 Schematic illustration of oil contact angle measurement after adding chemical additives (OH ⁻ , H ⁺ , NaOCl, and H ₂ O ₂) in aqueous solutions and diffusing process of chemical additives in aqueous film.....	20
Figure 4.3 The average value and standard deviation for oil CA on rock samples in treated and untreated brines/solutions	22
Figure 4.4 The gradual CA change of an oil droplet by adding (a) NaOH solution and (b) HCl solution in untreated NaCl solution, and (c) NaOH solution (d) HCl solution in untreated CaCl ₂ solution.....	25
Figure 4.5 The gradual CA change of an oil droplet by adding H ₂ O ₂ and NaOCl to (a & b) untreated NaCl solution and (c & d) untreated CaCl ₂ solution.....	26
Figure 4.6 Schematic illustration for cation bridging and ligand bridging between quartz and oil. Modified with permission from ref. 68. Copyright 2017, Elsevier	31
Figure 5.1 Amott cell used for soaking of oil-saturated core plugs in different soaking fluids. ..	36
Figure 6.1 Structure of PAM and HPAM (Gbadamosi et al., 2019)	43
Figure 7.1 Zetasizer Nano zs for particle size analysis.....	47
Figure 7.2 Anton Paar Rheometer MCR 302 for measuring dynamic viscosity and shear stress at different shear rate, and viscoelastic components G' (storage modulus) and G'' (loss modulus) at different angular frequency.....	48
Figure 7.3 The variation of a) shear stress and b) shear viscosity with shear rate for HPAM in DI water and FB	50

Figure 7.4 The picture of prepared HPAM solutions using a) DI water, b) FB	51
Figure 7.5 The hydrodynamic size of the HPAM molecules in a) DI water, b) FB	52
Figure 7.6 Viscoelastic properties at room temperature: storage and loss modulus of HPAM in DI water and FB with respect of angular frequency	54
Figure 8.1 The variation of shear viscosity and shear stress with shear rate for HPAM in a,b) NaCl, c,d) CaCl ₂ , e,f) MgCl ₂ , g,h) FeSO ₄ aqueous solutions	59
Figure 8.2 Picture of prepared HPAM solution for showing the stability of HPAM molecules in different aqueous solutions	63

Chapter 1 Introduction

1.1 Background

Increasing global energy demand from crude oil has led to an increase in water consumption in recent years. Water is heavily consumed in hydrocarbon extraction processes such as bitumen separation from mined oil sand, steam injection for in-situ oil sand recovery, enhanced oil recovery (EOR) for conventional oil extraction, and hydraulic fracturing in tight reservoirs. Alberta Energy Regulator (2019) reported that nearly 9.8 billion cubic meters (m^3) of water was used in Alberta in 2019. Of this, about 13% was used to develop energy resources, and the remainder was used in agriculture, forestry, and municipality sectors. In particular, the water consumption for energy extraction in 2019 included 1.004 billion m^3 for oil-sand mining, 0.256 billion m^3 for in situ oil sand recovery, 0.214 billion m^3 for EOR, and 0.024 billion m^3 for hydraulic fracturing.

The energy industry not only consumes a large amount of water but also produces a large volume of water during oil recovery operations. Produced water is a complex mixture of many organic and inorganic substances (al-Ghouti et al., 2019; Arthur et al., 2005; Fakhru'l-Razi et al., 2009), which is usually considered an oil field waste. It is either injected into disposal wells or recycled as an alternative water source (al-Ghouti et al., 2019). There are many challenges with disposal well injection. First, the produced brine needs to be transported and treated before injection into disposal wells (Igunnu and Chen., 2014). The costs associated with water disposal depend on the transportation distance and wastewater quality, ranging from \$1 to \$8 per barrel of water (EIA., 2016). Second, there is limited disposal capacity depending on location. The possible reasons include undeveloped disposal infrastructures and low injectivity for underground injection (Mccurdy., 2011). In the long term, increasing the disposal reservoir pressure may cause the

leakage of disposed water and result in underground water contamination (Igunnu and Chen., 2014).

Both environmental and economic concerns have driven research into the treatment of produced water. However, there are many practical limitations to the treatment and reuse of produced water. Generally, the major substances in produced water include (1) oil, polyaromatic hydrocarbons, benzene, toluene, ethylbenzene, xylenes, phenols, and organic acids that are naturally present in oil and gas formations; (2) surfactants, nanoparticles, polymers, scale and corrosion inhibitors, cross-linkers, and gel breakers that are added for different purposes; and (3) salts and heavy metals that are dissolved and suspended in water (al-Ghouti et al., 2019; Arthur et al., 2005). The presence of minerals and heavy metals (especially Fe) and the complex composition of produced water make the treatment process challenging.

1.2 Preview of the Study

The first part of the work studies the effects of the water treatment technology on rock–fluid interactions and rock wettability when the treated brine is reinjected into the reservoir. We first conduct contact-angle measurements by using treated and untreated synthetic formation brine (FB) and separate solutions of sodium chloride (NaCl), calcium chloride (CaCl₂), and sodium sulfate (Na₂S₂O₈) using the EO process to understand the impact of water treatment on rock wettability. We also conduct complementary experiments to measure the dynamic change in oil CA when oxidants, acid, and base are added to the untreated brine. Finally, spontaneous imbibition tests were conducted to compare the oil production using treated and untreated NaCl solutions to evaluate the effects of the treatment process on rock wettability.

In the second part of the study, we study the compatibility of untreated brine with friction reducer when reusing the produced FB to prepare the fracturing fluid. We first check the compatibility

between FB and friction reducer by measuring the dynamic (or shear) viscosity, hydrodynamic size of the HPAM, and viscoelasticity. Then, we investigate what ions in the brine cause the problem and what is the threshold concentration for those ions based on the dynamic viscosity results.

1.3 Objectives of Research

The objectives of this study are as follows:

- 1) Investigate the wetting characteristic difference when rock samples are soaked in treated and untreated brine.
- 2) Investigate which components in the treated brine change the rock wettability
- 3) Investigate if using the treated FB can enhance the oil recovery
- 4) Investigate the problems related to the reusing of untreated produced water to prepare the slickwater for hydraulic fracturing operation
- 5) Investigate the problematic ions and their threshold concentrations

1.4 Structure of Thesis

Chapter 1 briefly introduces the research background, research gap and objectives of this study.

Chapter 2 reviews previous studies on electro-oxidation (EO) technology and chemical interaction between rock and oxidants.

Chapter 3 presents the physical properties difference between untreated brine and treated brine by EO process.

Chapter 4 presents the results of static contact-angle (CA) measurements using treated and untreated brine, and the dynamic CA measurements by adding chemical additives to the untreated brine.

Chapter 5 presents the results of the spontaneous imbibition test on oil recovery using treated and untreated brine.

Chapter 6 introduces the background of using friction reducers and explains the research gap.

Chapter 7 compares the dynamic viscosity, particle size distribution and viscoelastic properties of HPAM in DI water and FB, and states the outcome of using untreated brine to prepare the slickwater.

Chapter 8 presents the results of dynamic viscosity of HPAM in different aqueous solution, and identify the problematic ions and their threshold concentrations.

Chapter 9 summarizes this study's main findings and provides recommendations for future studies.

Chapter 2 Literature Review of Water Treatment on Rock-fluid Interaction

2.1 Review of Water Treatment Methods

Various physical, chemical, and biological treatment processes can be combined for different treatment goals to reclaim the produced water. In general, three stages of treatment are followed to remove different contaminants from produced water (Ibrahim et al., 2013). In the primary stage, physical treatment is mainly applied to remove the remaining oil from produced water. A typical treatment process includes API separation, flocculation, and dissolved air flotation. After oil separation, the produced water will be subjected to secondary treatment to decompose waste organic matter. Biological treatment is the most cost-effective process for pollutant removal (Ibrahim et al., 2013). Dissolved organic matter (DOM) and microorganisms will be removed by hybrid physical and chemical treatment methods at the tertiary stage. At this stage, additional chemicals are added to coagulate micropollutants to improve the effluent quality further. Aggregated particles are then collected by filtration or activated carbon adsorption (Ibrahim et al., 2013). Other techniques can also accomplish the removal of petroleum contaminants, including electrochemical methods (Treviño-Reséndez et al., 2021; Bhagawan et al., 2016), membrane filtration (Rezakazemi et al 2018), photo-degradation (Alias et al., 2018), and advanced oxidation processes (Boczka and Fernandes., 2017; Ely et al., 2011).

2.2 Electro-oxidation Water Treatment Method

Electro-oxidation (EO) technology is a promising alternative for treating wastewaters containing organic pollutants. Generally, it is an electrochemical process where an electric field is applied on two special non-sacrificial electrodes (Ryan et al., 2021). The DOM will either be destroyed at the anode surface or degraded by generated oxidants (Pulkka et al.,2014). The EO process has the following advantages: (1) no additional chemicals are needed; (2) it breaks down and eliminates

both organic and inorganic contaminants (Petkov, 2014); (3) it eliminates wide range of bacteria, parasites, and viruses (Hand and Cusick 2021); and (4) it oxidizes heavy metals such as Cu, Zn, and Pb (Hu et al., 2021). The EO reactor cell also offers precipitation reactions on the cathode surface, where the divalent cations can be precipitated as carbonates and/or sulfates. The high pH environment on the cathode surface allows precipitation and crystallization of the precipitants. These unidirectional precipitation reactions hold these precipitants in the suspension as a suspended solid, and they do not have any affinity to amalgamate together or deposit on surfaces (Fraim and Jakhete., 2015). This makes the treated brine nonscaling without changing the total dissolved solids (TDS). The EO process thus provides a nonscaling and bacteria-free brine with oxidized heavy metals. In general, EO is a chemical-free, cost-efficient, and facile method, which generates strong oxidizing species by applying an external potential difference to the electrolyte solution.

Some studies reported successful implementation of the EO process for decontaminating oilfield-produced water. Up to 85% of petroleum hydrocarbon and 98% of chemical oxygen demand could be removed from produced water by a direct EO process (Rocha et al., 2012; dos Santos et al., 2014; Gargouri et al., 2014). Furthermore, the EO process generates multiple oxidants in the treatment reactor to oxidize organic and inorganic pollutants. Based on the ionic conditions of the water, oxygen-based oxidants such as peroxydisulfate ($S_2O_8^{2-}$), peroxydicarbonate ($C_2O_6^{2-}$), and hydrogen peroxide (H_2O_2), and chlorine-based oxidants such as active chlorine (Cl_2 , $HOCl$, and OCl^-) can be generated using the EO reactor cell (Ganiyu and Gamal El-Din., 2020), which could accomplish the goals of decontamination and disinfection (Fraim and Jakhete., 2015).

2.3 Chemical Interactions between Oxidants and Rock

The chemical interactions between oxidants and the rock have been discussed extensively. The previous investigations on oxidant–rock interactions have focused predominantly on permeability and pore connectivity improvement (Kuila et al., 2014; Chen et al., 2017; Zhou et al., 2018). This is because oxidants can easily dissolve chemically unstable components including DOM (Tamamura et al., 2015), chlorite, and pyrite (Evangelou and Zhang., 1995). For example, Yu et al. (2019) found that H_2O_2 can dissolve DOM in pores and pore throat under high temperature and pressure conditions, and the removal efficiency can be enhanced by increasing temperature, pressure, and reaction time. Chen et al. (2017) found that NaOCl, $Na_2S_2O_8$, and H_2O_2 can substantially dissolve carbonate, pyrite, chlorite, and organic matters, resulting in oxidation-induced fractures. Although extensive research has been carried out on permeability and pore connectivity improvement by oxidants, few studies investigated the performance of oxidants on rock wettability, especially the oxidants generated during the EO process. Numerous experimental studies have reported the impacts of reservoir rock wettability on oil recovery (Rostami et al., 2019; Alhammedi et al., 2017; Afekare et al., 2021; Al-Hadhrami et al., 2001; Kumar et al., 2020). The change in wettability of the reservoir rock to more water-wet conditions can improve oil recovery. For example, Lawal et al. (2022) observed that oil-aged calcite end pieces became more water-wet as the 3-pentanone concentration increased in brine based on their contact-angle experiments, while more oil was produced from core plugs as the 3-pentanone concentration increased based on their spontaneous imbibition tests. Kathel and Mohanty (2013) observed a significant improvement in oil recovery from low permeability sandstone samples during imbibition experiments when anionic surfactants were used to change rock wettability to more water-wet conditions. In this research, we propose that the oxidants produced by the EO process may dissolve

DOM on the rock surface, changing rock wettability to more water-wet conditions, thus leading to enhanced oil recovery.

2.4 Research Gaps

This work studies the effects of the EO process on rock–fluid interactions and rock wettability when the treated brine is reinjected into the reservoir. We hypothesize that the rock in the treated water is less oil-wet than that in the untreated one. To examine this hypothesis, we first treated different brine samples including synthetic formation brine (FB), and separate solutions of sodium chloride (NaCl), calcium chloride (CaCl₂), and sodium sulfate (Na₂SO₄) using the EO process. Then, we conducted contact-angle (CA) measurements to compare the wetting characteristics of the treated and untreated brine. We also conducted complementary experiments to measure the dynamic change in oil CA when oxidants, acid, and base are added to the untreated brine. Finally, spontaneous imbibition tests were conducted to compare the oil production using treated and untreated NaCl solutions to evaluate the effects of the treatment process on rock wettability.

Chapter 3 Effect of Electro-oxidation Process on Fluid Physical Properties

This section compares the physical properties, including density, surface tension, viscosity, and pH value of the water samples before and after the EO process. The oil-water interfacial tension between untreated and treated brine was also compared and studied. This section aims to understand the physical properties difference before and after the EO process.

3.1 Materials

3.1.1 Fluid Samples. The oil samples for IFT measurement were from the Montney Formation. The oil samples were filtered before conducting experiments using a 10- μm filter to remove possible impurities. The density and viscosity of the oil samples are 0.822 g/cm^3 and 3.24 cp, respectively. The surface tension of the oil is 22.3 mN/m.

The aqueous solutions used for experiments include synthetic FB, NaCl, CaCl₂, and Na₂SO₄ solutions with TDS of 90,000 and 45,000 ppm. The TDS of the original FB is 135,000 ppm, and its composition is presented in Table 3.1. The dominant ions in FB are Na⁺, Ca²⁺, and Cl⁻. The synthetic FB is then diluted to 90,000 and 45,000 ppm to conduct physical properties and oil-water IFT measurements. To understand the role of cations and anions on physical properties and oil-water IFT, we also used synthetic NaCl, CaCl₂, and Na₂SO₄ electrolyte solutions.

Table 3.1 Original ion composition of brine.

Ion	Na ⁺	K ⁺	Ca ²⁺	Mg ²⁺	Ba ²⁺	Sr ²⁺	Cl ⁻	HCO ³⁻	SO ₄ ²⁻
Concentration (mg/L)	37500	1370	10200	1290	34.8	838	82870	260	197.8

3.2 Methodology

3.2.1 EO Treatment. The EO process promotes the formation of oxidant species within the electrolyte solution. Chloride ion (Cl^-) is oxidized on the anode during the EO process to form chlorine gas (Cl_2). Then, Cl_2 reacts with water to form hypochlorous acid ($HOCl$) (Ganiyu & Martínez-Huitle, 2019). If sulfate ions are present in the brine, peroxydisulfate ($S_2O_8^{2-}$) would be generated during the EO process (Ganiyu & Gamal El-Din, 2020; Cañizares et al., 1944). On the cathode, H_2O_2 and hydroxyl ions (OH^-) are generated by reducing oxygen and water molecules (Chu et al., 2012). The electrochemical reactions that may occur on the anode (eqs 1 and 2) and the cathode (eqs 3, 4, and 5) are as follows:



The last reaction occurs in the presence of sulfate in the brine.

3.2.2 Surface Tension, Density, Viscosity, and Interfacial Tension Measurements. We measured the physical properties including density, surface tension (ST), viscosity, and pH of the brine before and after the treatment as well as the oil–water interfacial tension (IFT). A spinning drop tensiometer (SDT, Krüss, Germany) was used to measure IFT between oil and the aqueous fluids. The SDT device can measure IFT in the range of 10^{-6} to 2000 mN/m with an accuracy of

10–6 mN/m. The device has a capillary tube filled with the heavy phase and an end plug filled with the lighter phase. The rotational speed was set to 4500 rpm for all the tests (as shown in Figure 3.1). The solutions' ST and density were measured using an Attension Sigma 700 tensiometer (Biolin Scientific, Sweden) (as shown in Figure 3.2a). A Brookfield viscometer (DV2T, USA) was used to measure the viscosity of the fluids (as shown in Figure 3.2b).

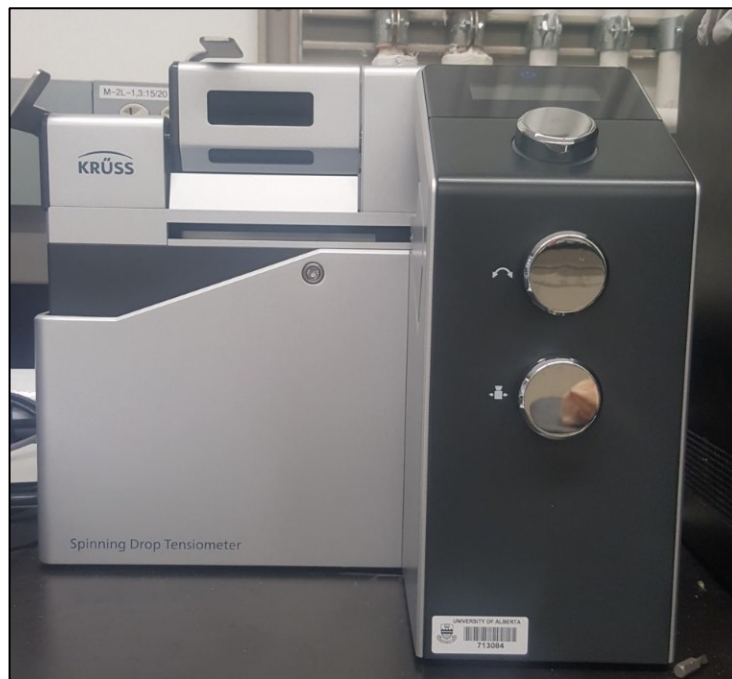
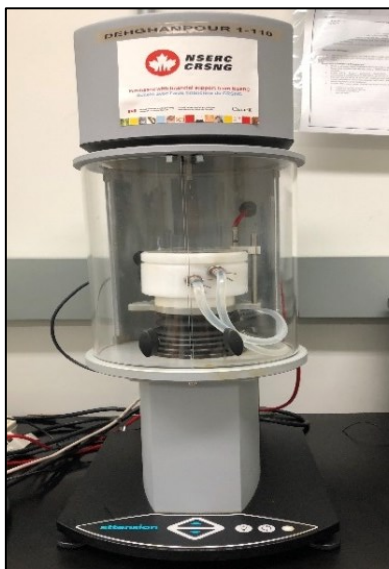
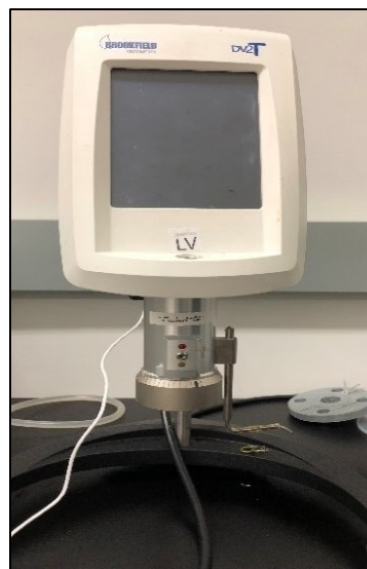


Figure 3.1 Spinning drop tensiometer.



(a)



(b)

Figure 3.2 The instrument used for physical properties measurements: (a) SIGMA 700 Tensiomer and (b) Brookfield Viscometer

3.3 Results and Discussion

3.3.1 Oxidants Generated by the EO Process.

After the EO process, active chlorine (Cl_2 , ClO^- , and HOCl), chlorine dioxide (ClO_2), and H_2O_2 are generated in the solutions. Table 3.2 lists the concentration of these oxidants before and after the EO process based on strip tests. There was no active chlorine, ClO_2 , and H_2O_2 in the initial brine, while after the EO treatment, these oxidants were detected at concentrations of 50–100 ppm, 0–10 ppm, and ~ 10 ppm, respectively. Figure 3.3 shows the concentration change of active chlorine and H_2O_2 versus time after the EO process to check the stability of each species in the aqueous solution. Note that the fate of ClO_2 and its impact on brine properties is not investigated in the present study because it is unstable in NaCl solutions (Medir & Giralt, 1982). From Figure 3.3a, it is observed that the active chlorine concentration in brine decayed significantly with time and reached 0 from an initial 100 ppm after 9 days, indicating that the generated active chlorine by the EO process was not stable in the brine. Len et al. (2002) reported a similar result of decaying

chlorine after the treatment and attributed it to the release of dissolved chlorine gas (Cl_2). On the other hand, the concentration of H_2O_2 only slightly reduced from 10 to 9 ppm after 3 days and then stayed constant for the next 6 days (Figure 3.3b), suggesting that H_2O_2 is stable in the treated water and could have a potential long-lasting impact on brine properties.

Table 3.2 Concentration difference of generated oxidants by EO process before and after treatment

Substances	Before Treatment	After Treatment
Active Chlorine (Cl_2 , HOCl , OCl^-)	0 ppm	50-100 ppm
Chlorine Dioxide (ClO_2)	0 ppm	0-10 ppm
Hydrogen Peroxide (H_2O_2)	0 ppm	~10 ppm

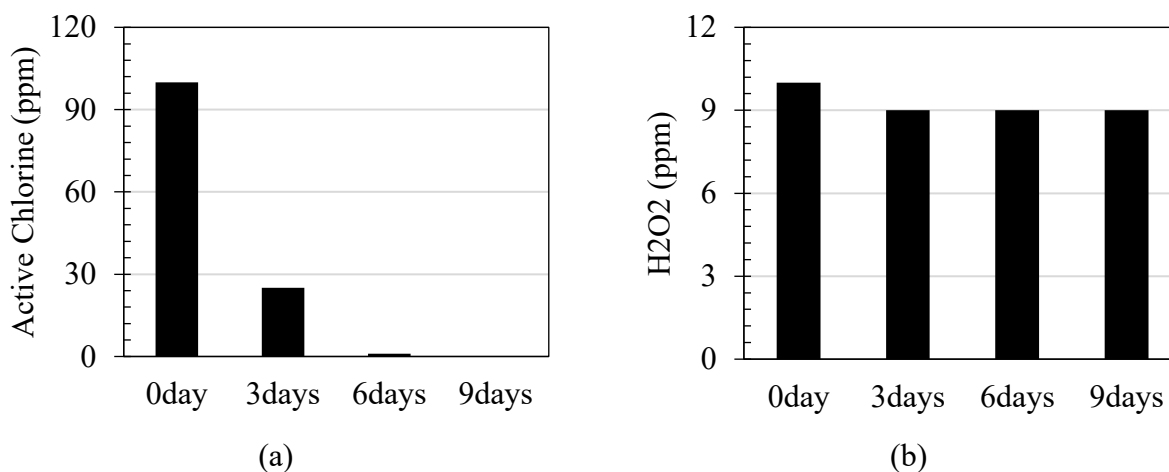


Figure 3.3 The concentration of (a) active chlorine and (b) H_2O_2 after 3, 6, and 9 days of the EO process. Note that active chlorine and H_2O_2 do not exist in untreated brine.

3.3.2 Effects of EO Treatment on the Physical Properties of Aqueous Solutions.

3.3.2.1 ST, Density, Viscosity, and pH Measurements. Table 3.3 lists the measured ST, density, viscosity, and pH of FB, NaCl, CaCl_2 , and Na_2SO_4 solutions with TDS of 90,000 and 45,000 ppm at room temperature ($25\text{ }^\circ\text{C}$) before and after the EO process. We observed that the ST, density, and viscosity of FB, NaCl, and CaCl_2 solutions were slightly reduced after the treatment. A likely

explanation is that FB, NaCl, and CaCl₂ solutions contain chloride ions, and the formation and dissolution of generated chlorine gas during the EO process (eqs 1 and 2) reduced the ST, density, and viscosity of the brine (Uhlig, 1937; De Ruiter, 2005). In contrast, no chlorine gas was produced after treating Na₂SO₄ solutions. Therefore, the ST, density, and viscosity of the Na₂SO₄ solution did not alter after the EO process. From this table, it is observed that the pH values of all solutions increased after the EO process, which can be due to the generation of hydroxyl ions at the cathode (eqs 4 and 5).

Table 3.3 The measured ST, density, viscosity, and pH of brine before and after the EO process

Fluid Sample	ST (mN/m)	Density (g/cc)	Viscosity (cp)	pH number
Untreated (UT) FB (90,000 ppm)	63.61±0.61	1.059±0.01	1.20±0.03	6.7±0.1
Treated FB (90,000 ppm)	57.70±0.17	1.021±0.01	1.13±0.02	7.7±0.1
UT FB (45,000 ppm)	61.54±0.61	1.039±0.01	1.17±0.03	7.6±0.1
Treated FB (45,000 ppm)	57.43±0.17	1.022±0.01	1.11±0.02	7.9±0.1
UT NaCl (90,000 ppm)	65.62±0.52	1.061±0.01	1.12±0.03	7.5±0.1
Treated NaCl (90,000 ppm)	58.73±0.38	1.032±0.01	1.07±0.02	8.5±0.1
UT NaCl (45,000 ppm)	62.46±0.52	1.056±0.01	1.11±0.03	7.2±0.1
Treated NaCl (45,000 ppm)	57.75±0.38	1.034±0.01	1.06±0.02	7.4±0.1
UT CaCl ₂ (45,000 ppm)	65.92±0.48	1.083±0.01	1.13±0.02	7.1±0.1
Treated CaCl ₂ (45,000 ppm)	59.32±0.37	1.056±0.02	1.09±0.03	7.6±0.1
UT Na ₂ SO ₄ (45,000 ppm)	64.75±0.36	1.067±0.01	1.11±0.03	8.2±0.1
Treated Na ₂ SO ₄ (45,000 ppm)	64.32±0.58	1.061±0.01	1.09±0.02	8.4±0.1

3.3.2.2 IFT Measurements. We also investigated the effect of different cations and anions on the oil–water IFT for treated and untreated aqueous solutions. The oil–water IFT results are summarized in Table 3.4. The pH values are also reported because there is a strong correlation between the oil–water IFT and pH.

Table 3.4 Summary of measured IFT between oil and treated/untreated brine.

	Oil-Untreated brine IFT (mN/m)	pH	Oil-Treated brine IFT (mN/m)	pH
90,000 ppm FB	21.79±0.56	7.6	22.54±0.76	7.8
45,000 ppm FB	21.72±0.34	7.6	22.14±0.45	7.9
90,000 ppm NaCl	15.36±0.22	7.5	14.05±0.10	8.5
45,000 ppm NaCl	12.85±0.25	7.2	14.57±0.99	7.4
45,000 ppm Na ₂ SO ₄	15.41±2.65	8.2	16.72±0.84	8.4
45,000 ppm CaCl ₂	13.31±0.14	7.1	14.59±0.29	7.6

As listed in Table 3.4, we observed that the IFT values between oil and treated aqueous solutions were slightly higher than the IFT values between untreated brine and oil, except for the case of 90,000 ppm NaCl solution. There are two likely causes for IFT reduction: (1) the change in the pH of the aqueous solution and (2) the generation of oxidants. We manually added chemical additives to the untreated aqueous solutions to investigate the effects of pH and the generated oxidants on IFT. The untreated 90,000 ppm NaCl solution with pH = 7.5 was used as the base case. The measured IFT values are listed in Table 3.5. As shown in this table, IFT values decreased significantly from 15.36 to 9.44 mN/m as the pH was increased from 7.5 to 8.5, while IFT values increased slightly from 15.36 to 16.5 mN/m when the pH was decreased from 7.5 to 5.5. Generally, oil–water IFT alteration with pH can be explained by dissociating acidic and basic functional groups on the oil surface (Watanabe & Iizuka, 1986). For example, Kelesođ lu et al. (2011) found that the oil–water IFT decreased by increasing the pH. They attributed this to the dissociation of acidic components (i.e., naphthenic acid dissociates to a carboxylate anion and H⁺), which

increased the solubility of the oil. Peter (1931) found that the oil–water IFT decreased by decreasing the pH due to the dissociation of basic components in oil. The maximum oil–water IFT value was found at near-neutral pH. In this case, the IFT value decreased either by increasing or decreasing the pH due to the dissociation of acidic or basic oil components (Bai et al., 2010; Pu et al., 2018). The generated active chlorine and H₂O₂ may also affect the IFT values. The oil–water IFT decreased to 4.15 mN/m after adding NaOCl, but it remained constant after adding H₂O₂ (15.51 ± 0.21 mN/m). The pH of brine increased to 9.7 after adding NaOCl. This is because the formation of HOCl also increases the concentration of OH⁻ (eq 7). We also evaluated the effects of HOCl by removing generated OH⁻ from brine. We added NaOCl to the brine and adjusted its pH to 7.5. As shown in Table 3.5, the oil–water IFT increased to 10.96 mN/m compared with the unadjusted one, indicating that HOCl can also reduce the oil–water IFT. Combining the results from Tables 3.4 and 3.5, we conclude that the opposite IFT results in the 90,000 ppm NaCl case are mainly due to pH differences after the EO process. Generally, there is no significant change in the oil–water IFT value before and after water treatment.

Table 3.5 The measured IFT values between oil and 90,000 ppm treated and untreated brine.

Fluid	IFT (mN/m)
Treated NaCl (pH 8.5)	14.03±0.10
Untreated (UT) NaCl (pH 7.5)	15.36±0.22
UT NaCl (pH 8.5)	9.44±0.24
UT NaCl (pH 5.5)	16.5±0.21
UT NaCl + NaOCl (pH 9.7)	4.15±0.19
UT NaCl + NaOCl (pH 7.5)	10.96±0.14
UT NaCl + H ₂ O ₂ (pH 7.5)	15.51±0.21

Chapter 4 Effect of Electro-oxidation Process on Tight-rock Wettability

This section presents CA measurements' results under limiting and dynamic conditions. Here we analyze the wettability of core samples in the presence of untreated brine and treated brine by EO process in limiting conditions to evaluate the wetting characteristic difference. Furthermore, we investigate the mechanism behind wettability alteration by adding chemical additives to untreated brine while observing CA change (dynamic conditions). This section aims to understand the rock wettability difference before and after the EO process.

4.1 Materials

4.1.1 Rock Samples. The rock samples in this study are collected from Montney Formation. Montney Formation is located in Alberta and British Columbia in Canada, containing approximately 13 trillion m³ of natural gas, 2.3 billion m³ of natural gas liquids, and 0.179 billion m³ of oil (Canada Energy Regulator, 2021). Four core plugs from four wells in the Montney Formation are used to conduct spontaneous imbibition tests. End pieces of core samples are collected for CA measurements.

The properties including porosity and permeability of the core plugs are listed in Table 4.1. The porosity of the plugs was measured by Boyle's law helium porosimetry method, which ranges from 5.04 to 6.52% of bulk volume. Permeability is measured by the pressure-decay method using helium gas, which ranges from 0.041 to 0.047 μ D. Table 4.2 lists the core plugs' mineralogy that is determined by X-ray diffraction (XRD) analysis. Our previous studies present more detailed properties of these core plugs (Yuan et al., 2019; Tran et al., 2021).

We use core end pieces to conduct the CA experiment. All end pieces were aged before conducting the experiments. First, we dried the rock end pieces in an oven at 90 °C to evaporate the initial oil and water in the pores. This can help us to eliminate the effect of initial fluid saturation on

wettability evaluation. Then, we placed the rock end pieces in a core holder filled with reservoir oil. The rock samples were aged in reservoir oil under an overburden pressure of 2000 psi for five days.

Table 4.1 Properties of the Montney core plugs used in this study.

Sample	Well	Depth (m)	Porosity (%)	Permeability (μ D)
1	1	2105.3	5.65	0.041
2	2	2125.6	5.04	0.047
3	3	2438.1	5.25	0.046
4		2468.0	6.52	0.043

Table 4.2 The mineralogy of the core plugs determined from XRD method.

Sample ID	Quartz (wt %)	K-feldspar (wt %)	Albite (wt %)	Calcite (wt %)	Dolomite (wt %)	Pyrite (wt %)	Total Clay (wt %)
1	56	9	10	N/A	17.2	1.5	5.3
2	48	12	9	N/A	8.6	4.3	17.9
3	60	8	10	N/A	13	1.8	7.4
4	58	8	11	N/A	17.7	1.3	5

4.1.2 Fluid Samples. The oil samples from the Montney Formation were filtered using a 10- μ m filter to remove possible impurities, which may affect the experimental results. The density and viscosity of the oil samples are 0.822 g/cm³ and 3.24 cp, respectively. The surface tension of the oil is 22.3 mN/m. The aqueous solutions used for experiments were same with the previous chapter, including synthetic FB, NaCl, CaCl₂, and Na₂SO₄ solutions with total dissolved solids (TDS) of 90,000 and 45,000 ppm.

4.2 Methodology

4.2.1 CA Measurements. The objectives of this measurement are to (1) confirm the wetting characteristic difference between EO treated brine and untreated brine and (2) investigate the influence of the individual species generated by the EO process on wetting properties. The core end pieces were polished using P220 sandpapers to get a smooth surface and then were saturated with oil for the CA measurements.

4.2.1.1 CA Measurements under Limiting Conditions. We first conducted CA tests to measure the equilibrated state of oil droplets in the presence of treated and untreated aqueous solutions. The oil droplets were released to equilibrate on the surface of the rock samples immersed in different aqueous solutions. Then, we used a high-resolution camera to visualize the profiles of the equilibrated oil droplets. The setup for contact angle measurements is shown in Figure 4.1. The detailed procedure for the CA measurements is provided in our earlier study (Yuan et al., 2021).

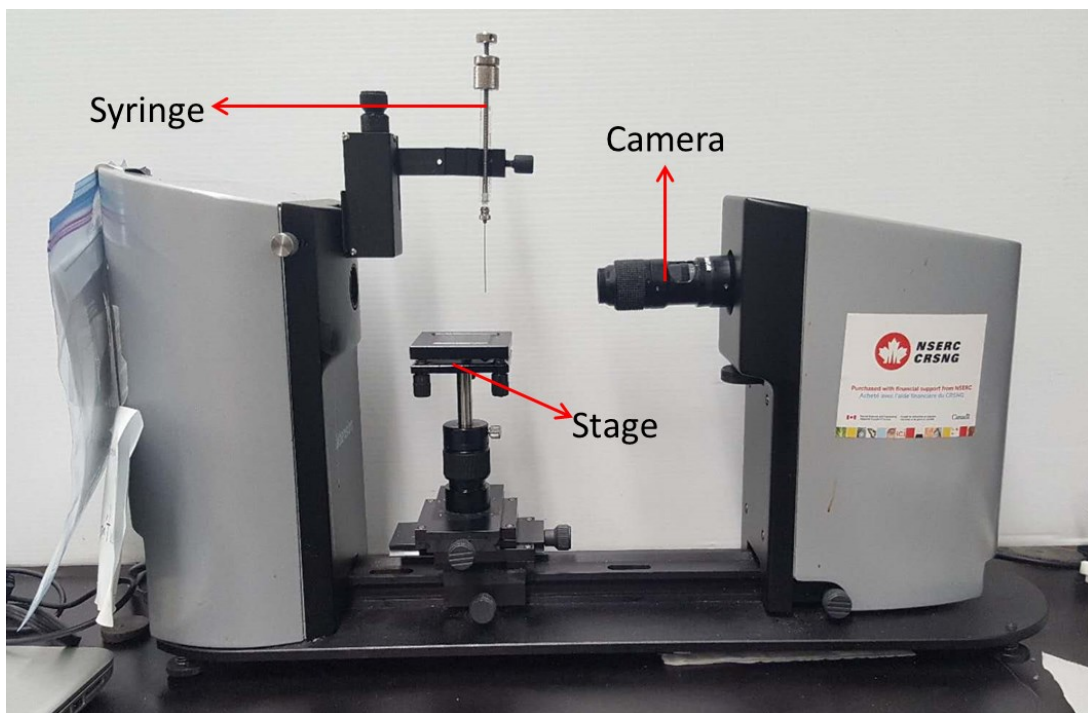


Figure 4.1 The instrument used for CA measurements

4.2.1.2 CA Measurements under Dynamic Conditions. After EO treatment, multiple chemicals can be generated, influencing the rock–fluid interactions and rock wettability. To identify the effects of generated chemicals (OH^- , H^+ , OCl^- , and H_2O_2) on real-time wettability change, we manually added NaOH, HCl, NaOCl, and H_2O_2 solutions to untreated brine and monitored the CA of oil droplets under dynamic conditions. First, we released an oil droplet to sit on the rock surface immersed in untreated brine. After the oil droplet was equilibrated, we slowly injected (0.5 mL/min) different chemical components (NaOH, HCl, NaOCl, and H_2O_2) into the untreated brine and measured the CA change during diffusion of these components toward the oil droplet until arriving at the equilibrium conditions. The diffusion of the chemical components to the oil/water/rock system is schematically illustrated in Figure 4.2. The CA change during the diffusion process reflects the effect of these chemicals on rock wettability. More details about this procedure can be found in our previous study (Yuan et al., 2021).

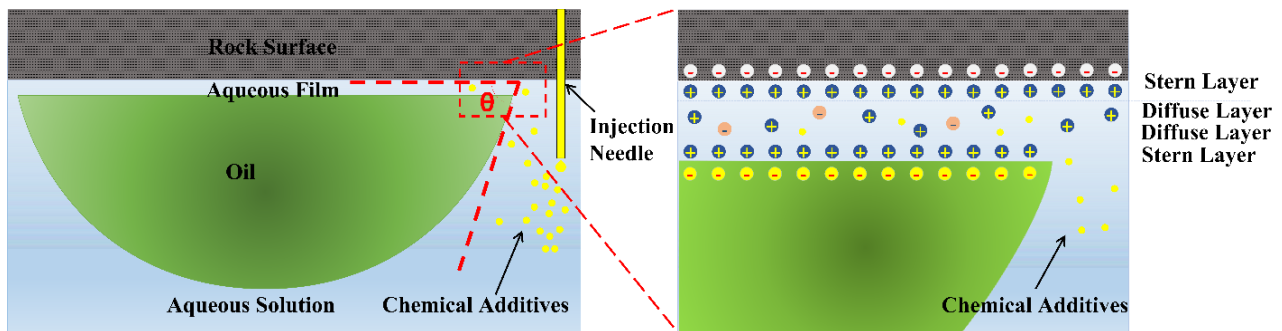


Figure 4.2 Schematic illustration of oil contact angle measurement after adding chemical additives (OH^- , H^+ , NaOCl, and H_2O_2) in aqueous solutions and diffusing process of chemical additives in aqueous film.

The volume and the concentration of injected chemicals are selected based on the final concentration of generated chemicals after the EO process and are presented in Table 4.3. NaOH and HCl solutions were added to the untreated solution to study the effect of pH on wettability. The impact of generated oxidants during the EO process was examined by adding 0.043 mL NaOCl

and 0.02 mL H₂O₂ solutions to the brine. The volume of these oxidants is calculated based on their final concentrations in the brine after the EO process (100 and 10 ppm for active chlorine and H₂O₂, respectively). We selected NaOCl as the source of active chlorine based on the following reaction:



The volume of chemical additives is much lower than the base liquid volume, and thus, the effects of liquid dilution on CA measurements are negligible.

Table 4.3 Concentration and volume of chemical additives added to the base aqueous solutions.

Chemicals	Volume (mL)
NaOH solution (pH 10.6)	0.4
HCl solution (pH 2.5)	0.4
NaOCl solution (13-15 wt%)	0.043
H ₂ O ₂ solution (3 wt%)	0.02

4.3 Results

4.3.1 Equilibrated CA under Limiting Conditions.

Here, we measured and compared the oil CAs equilibrated on the rock surface in the presence of treated and untreated aqueous solutions. Figure 4.3 shows the average CA results and standard deviations of 25 oil droplets for each treated and untreated aqueous solution on similar rock end pieces under ambient temperature and pressure. The variations of CA measurements are mainly due to the heterogeneity of the rock and aging time (Silveira et al., 2022; Fernø et al., 2002; Graue et al., 2002).

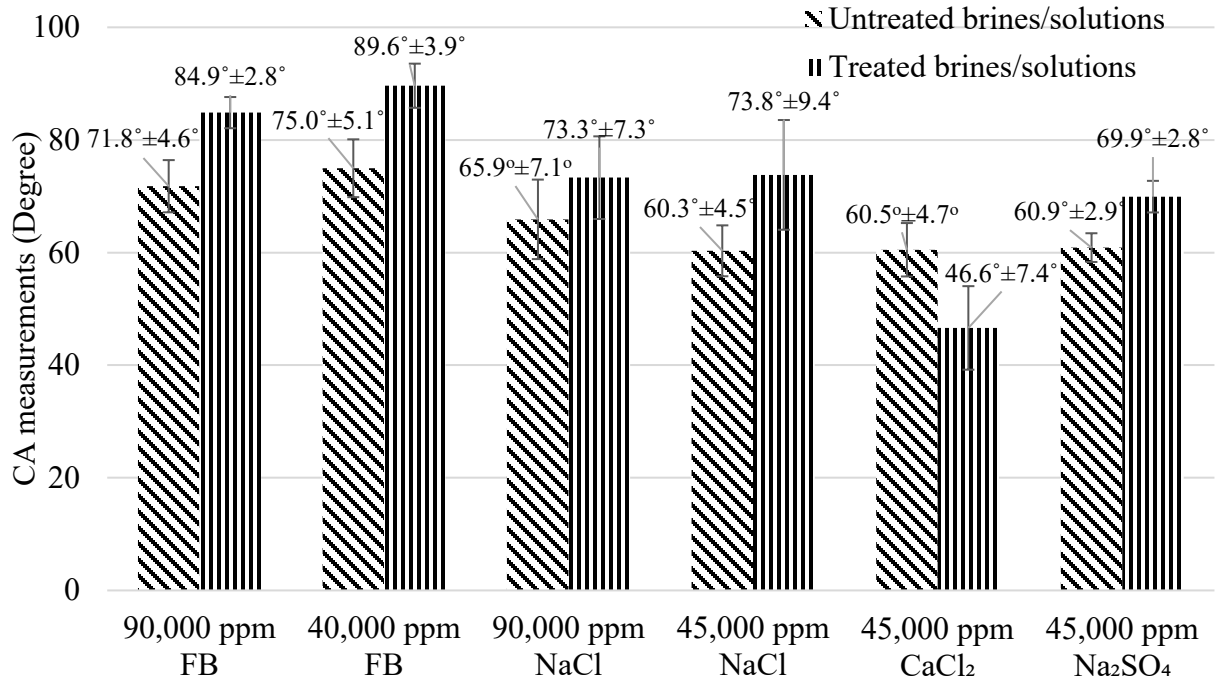


Figure 4.3 The average value and standard deviation for oil CA on rock samples in treated and untreated brines/solutions

As shown in Figure 4.3, the oil CAs in untreated FB of 90,000 and 45,000 ppm are $71.8^{\circ} \pm 4.6^{\circ}$ and $75.0^{\circ} \pm 5.1^{\circ}$, while those in treated FB of 90,000 and 45,000 ppm are $84.9^{\circ} \pm 2.8^{\circ}$ and $89.6^{\circ} \pm 3.9^{\circ}$, respectively. Similar CA results are observed in 90,000 and 45,000 ppm NaCl solutions. The CAs in untreated NaCl solution of 90,000 and 45,000 ppm are $65.8^{\circ} \pm 7.1^{\circ}$ and $60.3^{\circ} \pm 4.5^{\circ}$, while those in treated NaCl solution are $73.3^{\circ} \pm 7.3^{\circ}$ and $73.8^{\circ} \pm 9.4^{\circ}$, respectively. These results suggest that the rock surface is less oil-wet when exposed to treated FB and NaCl solution compared to untreated FB and NaCl solution. Moreover, the similar values of average and standard deviations for CA between the two salinity cases imply that salinity does not significantly affect the wettability of the rock surface in our experiments.

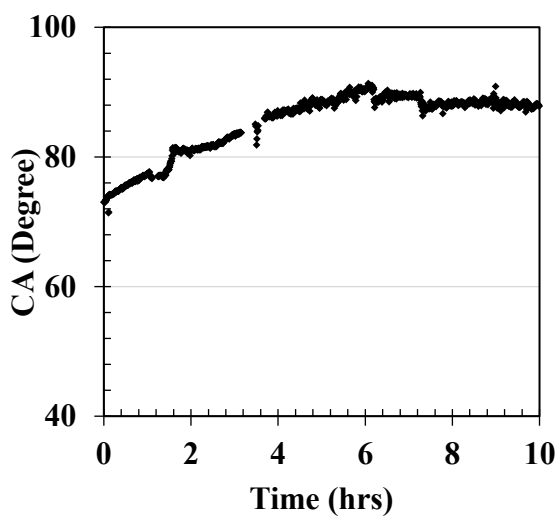
We also investigated how anion and cation types influence the wettability of the rock in untreated and treated aqueous solutions. As can be observed in Figure 4.3, the oil CAs on the rock exposed to untreated NaCl, CaCl₂, and Na₂SO₄ solutions are $60.3^{\circ} \pm 4.5^{\circ}$, $60.5^{\circ} \pm 4.7^{\circ}$, and $60.9^{\circ} \pm 2.9^{\circ}$,

respectively. The similar values of CA in the untreated solutions suggest that the anion and cation types do not influence the CA results significantly in untreated aqueous solutions. However, we observed different CA results in treated aqueous solutions with different salts. The oil CA values in treated NaCl and Na₂SO₄ solutions are $73.8^\circ \pm 9.4^\circ$ and $69.9^\circ \pm 2.8^\circ$, respectively, which are higher than the CA values in untreated cases. These results show that the rock samples exposed to treated NaCl and Na₂SO₄ solutions are more water-wet than those exposed to untreated cases. However, oil CA in the treated CaCl₂ ($46.6^\circ \pm 7.4^\circ$) solution is lower than that in the untreated CaCl₂ ($60.5^\circ \pm 4.7^\circ$) solution, suggesting that the rock is more oil-wet in the treated CaCl₂ solution. Note that the fluid properties and IFT values do not significantly change before and after the EO process for all the aqueous solutions, but the oil CA values in treated CaCl₂ are different from those in other cases that will be discussed later in this paper.

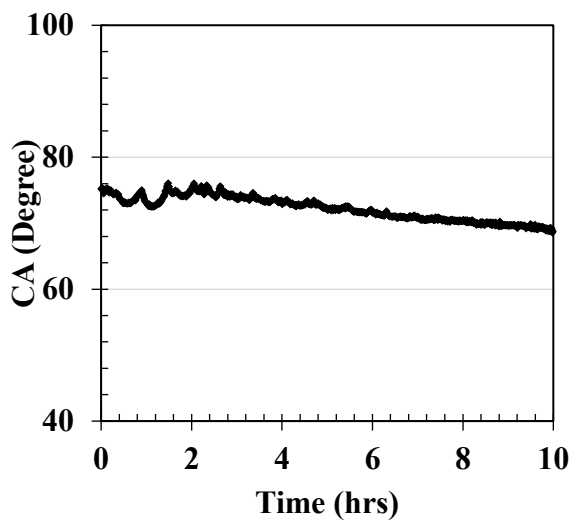
4.3.2 Change in Oil CA upon the Addition of OH⁻, H⁺, and Oxidants. The results of oil CA tests under limiting conditions show that the rock in the treated FB, NaCl, and Na₂SO₄ solutions is less oil-wet than that in the untreated cases, and the rock in the treated CaCl₂ solution is more oil-wet than that in the untreated one. We hypothesize that the difference in wetting characteristics for treated and untreated aqueous solutions is due to the generated oxidants. To evaluate the influence of generated oxidants, we conducted special tests to investigate the change in CA with time during the diffusion of the chemical additives toward an oil droplet initially equilibrated on the rock surface. The CA change is then monitored during the diffusion process. The limiting CA data presented in the previous section had uncertainties due to rock heterogeneity and aging time. However, in the dynamic CA tests, the effects of rock heterogeneity and oil-droplet size and shape are negligible since the CA change of a single oil droplet is observed over the course of the experiment. Therefore, the observed change in CA is mainly due to the added individual chemicals.

Also, since the injection rate of chemical additives is slow, the hydrodynamic force should be negligible in these experiments.

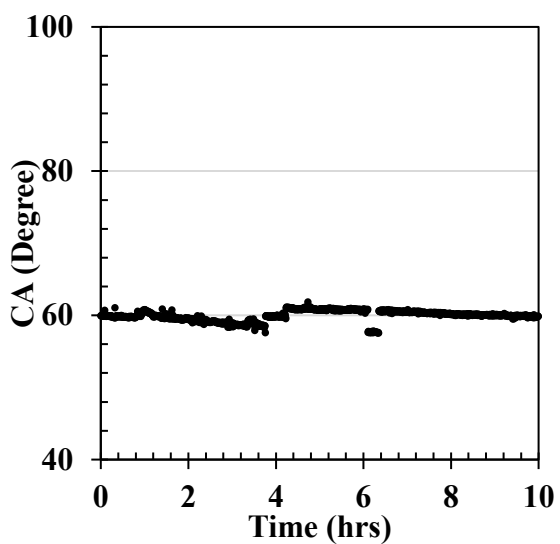
4.3.2.1 CA Change upon the Addition of NaOH and HCl. After the EO process, the pH of the brine slightly increases compared with the initial pH value (as shown in Table 3.3). To study how the pH change affects the oil CA, we first exposed the rock end piece to 60 mL of untreated brine and then released an oil droplet on the rock surface using a J-shape needle. When the oil droplet was stabilized, we added 0.4 mL of NaOH (pH = 10.6) or HCl (pH = 2.5) solution into untreated brine and recorded the CA change to study the effects of OH^- and H^+ on wettability change. Figure 4.4a shows the dynamic change in CA during NaOH diffusion in a NaCl solution. We observed that the initial oil CA was 73° , and it gradually increased to 87° , indicating that adding NaOH changed the rock wettability toward less oil-wet conditions. Figure 4.4b shows the CA change in the NaCl solution during HCl diffusion. The oil CA was initially 75° , and it gradually decreased to 69° , indicating that adding HCl led to more oil-wet conditions. Figure 4.4cd show the change in CA of an oil droplet in the presence of CaCl_2 solution when adding NaOH and HCl, respectively. Both oil droplets initially had a CA of 60° in these two cases, which remained relatively constant for 10 h. The HCl and NaOH diffusion results indicate that the pH has no influence on the oil CA in the presence of CaCl_2 solution.



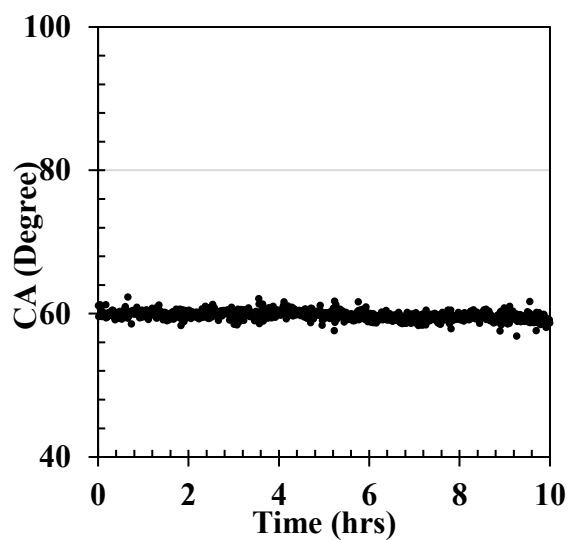
(a)



(b)



(c)



(d)

Figure 4.4 The gradual CA change of an oil droplet by adding (a) NaOH solution and (b) HCl solution in untreated NaCl solution, and (c) NaOH solution (d) HCl solution in untreated CaCl_2 solution.

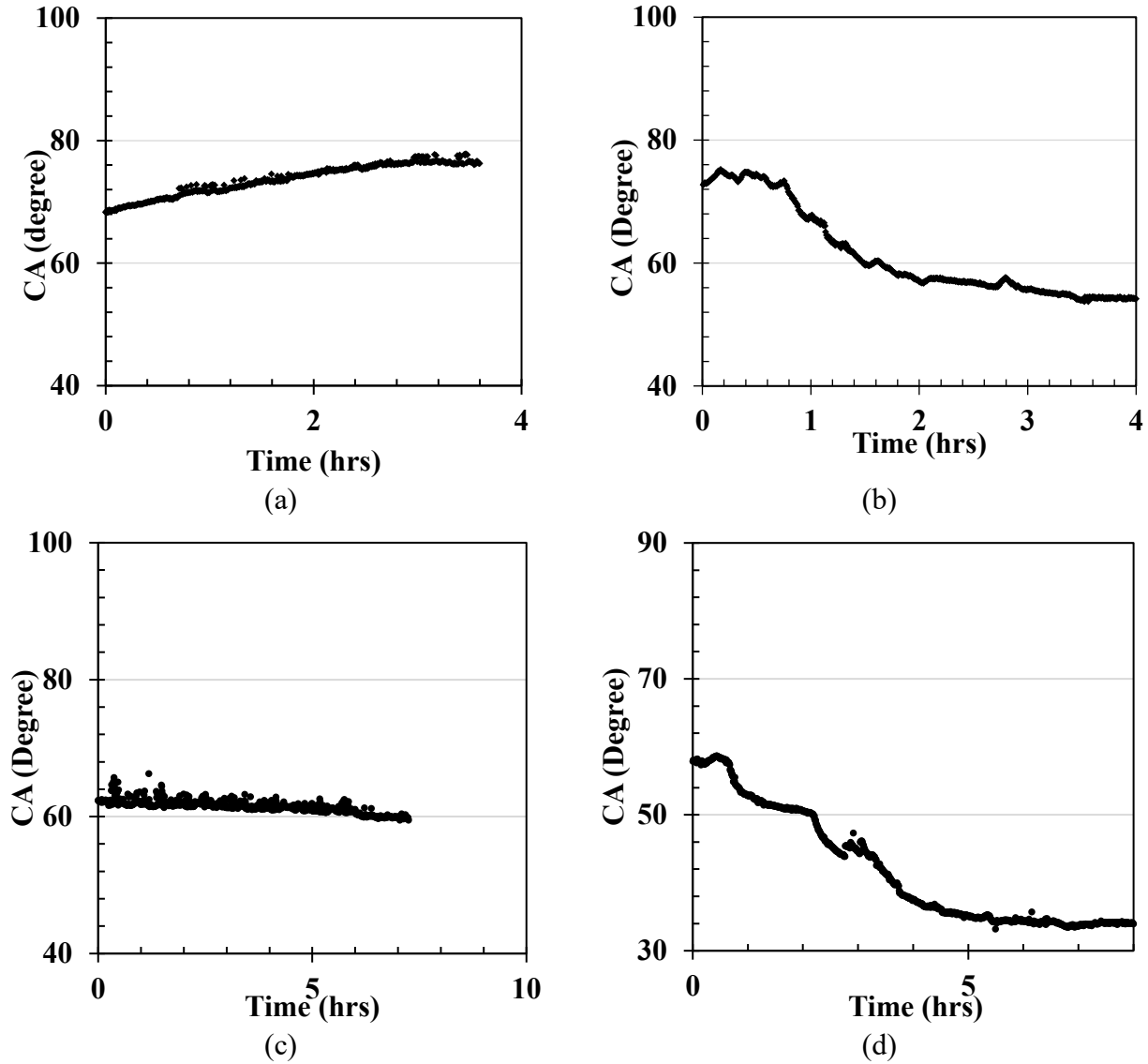


Figure 4.5 The gradual CA change of an oil droplet by adding H_2O_2 and $NaOCl$ to (a & b) untreated $NaCl$ solution and (c & d) untreated $CaCl_2$ solution.

4.3.2.2 CA Change upon the Addition of H_2O_2 . H_2O_2 is one of the oxidants generated in the EO process. The concentration of H_2O_2 after the EO treatment is around 10 ppm, as shown in Table 3.2. Therefore, we added 0.02 mL of 3 wt % H_2O_2 solutions in 60 mL of untreated brine to make the final concentration of H_2O_2 to about 10 ppm. Figure 4.5a shows the CA change of the oil droplet initially equilibrated on a rock sample during H_2O_2 diffusion in an untreated brine. We

observed that the initial oil CA was around 68° , and it gradually increased to 76° and stabilized after 3 h. This observation suggests that H_2O_2 can make the rock surface more water-wet. Similarly, the same amount of H_2O_2 was added to the untreated CaCl_2 solution for the dynamic CA measurement (Figure 4.5c). The oil on the rock surface had an initial CA of about 62° , and the CA was almost constant in the next 7 h. The insignificant CA change during the diffusion of H_2O_2 indicates that H_2O_2 cannot change the rock wettability in the CaCl_2 solution.

4.3.2.3 CA Change upon the Addition of Sodium Hypochlorite. Active chlorine is another product of the EO process. In the experiments, 0.043 mL of 13–15 wt % NaOCl solution was added to 60 mL of untreated brine to reach the final active chlorine concentration of 100 ppm. Figure 4.5b shows how the oil CA changes during the NaOCl diffusion toward the oil droplet. The initial oil CA was 72° , and it gradually decreased to 55° after 4 h, suggesting that active chlorine can change the rock wettability toward more oil-wet conditions. Note that the pH of the brine after adding NaOCl reached 9.7. As mentioned above, the oil CA increased by increasing the pH, which seems counterintuitive as the oil CA decreases significantly after adding NaOCl . A similar CA experimental result was obtained in the CaCl_2 solution (Figure 4.5d). The oil CA gradually decreased from 58 to 34° in the first 4 h and stayed constant for 4 h. Therefore, the lower oil CA in the treated CaCl_2 solution compared with the untreated CaCl_2 solution under limiting conditions (Figure 4.3) can be explained by the generation of active chlorine in the treated CaCl_2 solution.

4.4 Discussion

4.4.1 Effect of pH on CA Change. The observation that CA changes with pH in NaCl solutions can be explained by the Derjaguin–Landau–Verwey–Overbeek (DLVO) theory. DLVO theory uses attractive van der Waals (vdW) and repulsive electrostatic interaction (EDL) forces to estimate the hydrophilicity of a surface (Israelachvili, 2011; Sanaei et al., 2019). The EDL force

is typically stronger than the short-range vdW forces. In our experiments, high-salinity aqueous solutions (90,000 and 45,000 ppm) were used as the base liquids. Therefore, a thin electric double layer is expected to form due to the high ionic strength of the solution that creates a condition favoring the attachment of oil to the rock (Israelachvili, 2011). Therefore, in all experiments, the CA was less than 90° . While the high ionic strength of base solutions in the present study has mitigated the electrostatic repulsive interaction, the alteration of the EDL force at different experimental conditions is still significant, as implied in Figures 4.3, 4.4, and 4.5. The EDL force is directly related to the surface charge, which is significantly influenced by the solution pH. As the pH increases, the charge density of negatively charged surfaces increases (Wang et al., 2016). This can be explained by the dissociation reactions of the chemical species on oil and rock surfaces. Table 4.4 lists the chemical reactions and equilibrium constant values at 25°C for oil–water and rock–water interfaces. The surface chemical species can influence the surface energy and thus surface potential (Zeng et al., 2019). At the oil–water interface, the functional groups on the oil surface dissociate and form charged functional groups such as quaternary ammonium ($\text{R} - \text{NH}^{3+}$) and carboxylates ($\text{R} - \text{COO}^-$) (Brady et al., 2012). On increasing the water pH, H^+ reacts with OH^- , and the first two reactions in Table 4.4 progress to the right (forward). The deprotonation of $\text{R} - \text{NH}^{3+}$ and $\text{R} - \text{COOH}$ is thus promoted, and the concentration of $\text{R} - \text{NH}^{3+}$ decreases and that of $\text{R} - \text{COO}^-$ increases consequently. Therefore, the reduction in the $\text{R} - \text{NH}^{3+}$ concentration and the increase in the $\text{R} - \text{COO}^-$ concentration make the oil more negatively charged. In our rock samples, the minerals include quartz, feldspar, calcite, dolomite, and clays. $>\text{SiOH}$ is the Si group exposed on the quartz surface, while $>\text{CaOH}$ and $>\text{CO}_3\text{H}$ represent the calcium and carbonate groups on the calcite or dolomite surface (Brady et al., 2012; Brady and Krumhansl, 2012). The quartz content is more than 40% in our rock samples. When the pH is more than 3.0 (the typical

isoelectric point of quartz), the surface of quartz is negatively charged (Dong and Wan, 2014). When the pH increases, $>\text{SiO}^-$ increases due to the equilibrium shift to the right side and deprotonates more SiOH. The hydroxyl groups $>\text{AlOH}$ and $>\text{SiOH}$ represent the hydroxylated Al and Si groups exposed at the edge of clay minerals, which can adsorb cations or anions (Gu and Evans, 2007). For the clay mineral, as the pH increases, $>\text{AlOH}$ and $>\text{SiOH}$ tend to deprotonate and lead to the increase of $>\text{AlO}^-$ and $>\text{SiO}^-$. Therefore, both rock and oil surfaces become more negatively charged, and the EDL repulsion between the two interfaces increases, leading to a less oil-wet condition.

4.4.2 Effect of Cation Bridging on CA. The calcium ion-bridging effect can explain why the CA does not change with pH in CaCl_2 solutions in the water film. The ion-bridging effect describes the chemical interactions between oil and the rock in the oil/brine/rock system, which are caused by divalent cations (Hu et al., 2021). In particular, divalent cations (e.g., Ca^{2+} and Mg^{2+}) form hydrated cations (e.g., $[\text{Ca}(\text{H}_2\text{O})_6]^{2+}$ and $[\text{Mg}(\text{H}_2\text{O})_6]^{2+}$) in the water film. These hydrated cations can bridge the negatively charged polar components (e.g., carboxyl, hydroxyl, and phenols) on the crude oil surface and the negatively charged sites on the rock surface (e.g., $>\text{SiO}^-$ and $>\text{AlO}^-$), providing attraction between rock and oil surfaces (Wang et al., 2020). Monovalent cations (e.g., Na^+ and K^+) also form hydrated cations in the water film (Brady et al., 2012), but the strength of divalent cation bridging is much stronger than that of monovalent cations due to their larger hydration capacity (Kobayashi et al., 2017). Tian et al. (2019) compared the strength of monovalent cation bridging, divalent cation bridging, and EDL repulsion at low, medium, and high ionic strengths. They found that divalent cation bridging has the most substantial impact on enhancing oil-wetness regardless of ionic strength, and monovalent cation bridging has the weakest effect on improving oil-wetness regardless of ionic strength. A ligand bridging would

form if multivalent ions simultaneously connect both rock and oil with ligands, as shown in Figure 4.6. The strength of ligand bridging is typically more significant than cation bridging (Tian and Wang, 2019). The cation bridging and ligand bridging formed between oil and rock are shown in Figure 4.6. In our CA measurements, both cation bridging and ligand bridging are expected to form between rock and oil in a CaCl_2 solution due to the high concentration of Ca^{2+} . Therefore, the binding strength between oil and rock is high enough to eliminate the effect of pH on EDL repulsion.

Table 4.4 The interaction and equilibrium constant at 25°C for oil-water and rock-water interfaces (Sanaei et al., 2019; Zeng et al., 2019). (- for the oil phase and > for rock surface)

Reaction	Log $K_{25^\circ\text{C}}$
Oil-water interface	
$R - \text{NH}_3^+ \leftrightarrow R - \text{NH}_2 + \text{H}^+$	-6.0
$R - \text{COOH} \leftrightarrow R - \text{COO}^- + \text{H}^+$	-5.0
$R - \text{COOH} + \text{Ca}^{2+} \leftrightarrow R - \text{COOCa}^+ + \text{H}^+$	-3.8
$R - \text{COOH} + \text{Mg}^{2+} \leftrightarrow R - \text{COOMg}^+ + \text{H}^+$	-4.0
Rock-water interface	
Quartz-water interface	
$> \text{SiOH} \leftrightarrow > \text{SiO}^- + \text{H}^+$	-4.0
$> \text{SiOH} + \text{Ca}^{2+} \leftrightarrow > \text{SiOCa}^+ + \text{H}^+$	-9.7
$> \text{SiOH} + \text{CaOH}^+ \leftrightarrow > \text{SiOCaOH} + \text{H}^+$	-4.5
Calcite-water interface	
$> \text{CaOH} + \text{H}^+ \leftrightarrow > \text{CaOH}_2^+$	11.8
$> \text{CaOH} + \text{HCO}_3^- \leftrightarrow > \text{CaOH}_2^-$	5.8
$> \text{CO}_3\text{H} \leftrightarrow > \text{CO}_3^- + \text{H}^+$	-5.1
$> \text{CO}_3\text{H} + \text{Ca}^{2+} \leftrightarrow > \text{CO}_3\text{Ca}^+ + \text{H}^+$	-2.6
$> \text{CO}_3\text{H} + \text{Ca}^{2+} \leftrightarrow > \text{CO}_3\text{Ca}^+ + \text{H}^+$	-2.6
Clay (kaolinite)-water interface	
$> \text{AlOH}_2^+ \leftrightarrow > \text{AlOH} + \text{H}^+$	-3.0
$> \text{AlOH} \leftrightarrow > \text{AlO}^- + \text{H}^+$	-3.8
$> \text{SiOH} \leftrightarrow > \text{SiO}^- + \text{H}^+$	-7.0
$> \text{AlOH} + \text{Ca}^{2+} \leftrightarrow > \text{AlOCa}^+ + \text{H}^+$	-9.7
$> \text{SiOH} + \text{Ca}^{2+} \leftrightarrow > \text{SiOCa}^+ + \text{H}^+$	-9.7
$> \text{AlOH} + \text{CaOH}^+ \leftrightarrow > \text{AlOCaOH} + \text{H}^+$	-4.5
$> \text{SiOH} + \text{CaOH}^+ \leftrightarrow > \text{SiOCaOH} + \text{H}^+$	-4.5

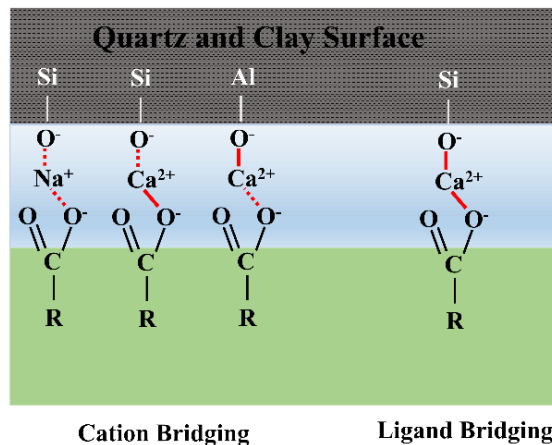


Figure 4.6 Schematic illustration for cation bridging and ligand bridging between quartz and oil. Modified with permission from ref. 68. Copyright 2017, Elsevier

4.4.3 Effect of Oxidants on CA. The presence of oxidants (e.g., H₂O₂, NaOCl, and Na₂S₂O₈) in the brine can result in the dissolution of the organic matter and minerals such as pyrite and chlorite (Chen et al., 2017; Zhou et al., 2018; Yang et al., 2020; Chen et al., 2018). The mechanism of the dissolution of DOM by oxidants is degrading the long-chain organic molecules to soluble organic molecules (Liu et al., 2013a; Liu et al., 2013b). Yang et al. (2020) compared the removal efficiency of DOM by NaClO, Na₂S₂O₈, and H₂O₂. They found that NaOCl is the most effective oxidant and H₂O₂ is the weakest oxidant in DOM removal. The dissolution of the DOM by oxidants can lead to the rock being more water-wet (Cheng et al., 2021). Mineral dissolution also occurs when oxidants are present in aqueous solutions. Oxidants can oxidize the inorganic minerals such as carbonate, clay minerals, and quartz in acidic/basic environments. Li et al. (2020) studied the mineral–oxidant interactions by conducting oxidative dissolution experiments. They found that the rock mass reduces after treating rock samples with H₂O₂ and Na₂S₂O₈, while it reduces first and then increases over time when treating rock samples with NaOCl. They explained that the mass loss is due to the mineral dissolution (e.g., pyrite and carbonate in the acidic environment

and quartz, albite, illite, and chlorite in the alkaline environment), and mass gain is due to the precipitation of metal (e.g., Ca^{2+} , Mg^{2+} , Al^{3+} , and Fe^{3+}) hydroxides that are produced from NaOCl–mineral reactions in the alkaline environment. They also monitored the concentration of different cations while using oxidants to treat their rock sample. They found that using NaOCl to treat the rock significantly increases the concentration of Fe^{3+} , K^+ , Ca^{2+} , Mg^{2+} , and Al^{3+} , using H_2O_2 only increases the concentration of Ca^{2+} and Fe^{3+} , and using $\text{Na}_2\text{S}_2\text{O}_8$ increases the concentration of K^+ and Al^{3+} . Note that the precipitation of minerals is not considered in the CA experiments since the mineral precipitation in the first 10 h is very limited and can be ignored (Li et al., 2020). Based on the CA results shown in Figure 4.5, oil CAs reduced upon the addition of NaOCl in both NaCl and CaCl_2 solutions, suggesting that NaOCl can make the rock more oil-wet. NaOCl is a strong oxidant that can oxidize DOM and minerals (pyrite and chlorite) in alkaline environments (Kuila et al., 2014). Upon injection of NaOCl in NaCl and CaCl_2 solutions, pyrite tends to dissolve into the aqueous solution, and the concentration of Fe^{3+} increases. Moreover, a high pH value (pH = 9.7), triggered by the addition of NaOCl, enhances the alkali–silica reaction, leading to the dissolution of quartz, feldspar, and clay minerals and release of high-valence cations (e.g., Mg^{2+} , Si^{2+} , Ca^{2+} , Al^{3+} , or Fe^{3+}) into the aqueous solution (Thomas, 2011). The release of these high-valence cations can lead to a stronger bridging between rock and oil than the low valence cations (Tunega et al., 2014), increasing the rock–oil attraction and changing the rock wettability toward more oil-wet conditions. At the same time, the dissolution of DOM also occurs after the diffusion of NaOCl in the base cases, resulting in a more water-wet rock surface. Nevertheless, multivalent bridging likely affects the oil/water/rock system more significantly than the DOM dissolution because a reduced CA (more oil-wet) was observed after the addition of NaOCl to the aqueous solution. The CA results show that the rock becomes more water-wet when

H₂O₂ is added to the NaCl solution. Both mineral (pyrite and chlorite) dissolution and DOM dissolution can occur upon the addition of H₂O₂ to the aqueous solutions. The increased oil CA (more water-wet) suggests that DOM dissolution is more dominant in the system than mineral dissolution. However, H₂O₂ cannot change the oil CA in the CaCl₂ solution, more likely due to a strong Ca²⁺ bridging between oil and rock in the CaCl₂ solution that protects the DOM from oxidation reactions (Feng et al., 2005; Kunhi Mouvenchery et al., 2012). In the limiting CA tests, the CA in the treated NaCl is higher than that in the untreated NaCl. This is because the EO process does not increase the pH as much as upon the addition of NaOCl to the aqueous solution. Therefore, the mineral dissolution from the alkali–mineral interaction is limited (Thomas, 2011), and oxidation of DOM by H₂O₂ and active chlorine becomes dominant, leading to more water-wet conditions. The CA in treated CaCl₂ is lower than that in untreated CaCl₂ in the limiting CA experiment, suggesting that the effect of mineral dissolution by oxidants is more dominant than that of DOM dissolution. This may also be due to the additional protection of DOM provided by Ca²⁺ bridging. In other words, the dissolution of DOM by oxidants between oil and rock is inhibited because of the Ca²⁺ bridging effect. Thus, the rock cannot become more water-wet. However, the dissolution of minerals by oxidants releases more high-valence cations (e.g., Mg²⁺, Si²⁺, Ca²⁺, Al³⁺, or Fe³⁺) into the solution, enhancing the bridging effect and leading to more attraction between oil and rock. The impact of the high-valence cations has been exemplified in a study by Haugen (2016) and Fjelde et al. (2017). Haugen (2016) found that the presence of Fe³⁺ in the brine can alter the wettability of the rock to more oil-wet conditions, and it had more significant impact on wettability than Ca²⁺ when the concentrations of the cations are the same. Fjelde et al. (2017) investigated the effect of cation bridging by Fe³⁺ on the rock wettability, and

they observed that a Fe^{3+} concentration as low as 50 ppm could alter the wettability of clay to more oil-wet conditions.

Chapter 5 Effect of Electro-oxidation on the spontaneous imbibition

This section presents the results of spontaneous imbibition tests. Here we analyze the oil production from two different core samples from the Montney formation in the presence of brine before and after the EO process. Moreover, we repeat the experiments with untreated brine + oxidants to check if similar results can be observed. The objective of this section is to check if more oil can be produced using treated brine by the EO process, since the rock wettability changing to a more water-wet condition is observed by using treated FB in Chapter 4.

5.1 Materials

5.1.1 Rock Samples. We use core samples in Table 4.1 and 4.2 to conduct the spontaneous imbibition tests. All core samples were aged before conducting the experiments. First, we dried the core samples in an oven at 90 °C to evaporate the initial oil and water in the pores. This can help us to eliminate the effect of initial fluid saturation on imbibition oil recovery experiments. Then, we placed the core samples in a core holder filled with reservoir oil. The core samples were aged in reservoir oil under an overburden pressure of 2000 psi for five days.

5.1.2 Fluid Samples. We use same oil sample (discussed in chapter 3) to conduct the spontaneous imbibition tests. We selected NaCl solution as soaking fluid because Na^+ and Cl^- are the major ions in the FB, as shown in Table 3.1.

5.2 Methodology

5.2.1 Spontaneous Imbibition Tests. We used treated and untreated aqueous solutions to conduct spontaneous imbibition tests and compare the imbibition oil recovery of different cases. We measured and compared the final oil recovery from two similar cores when they were soaked in (1) treated and untreated NaCl solutions and (2) untreated NaCl with and without oxidants. Similar

core plugs were obtained by cutting a long core sample in half. Therefore, these two cores' physical properties, including porosity, permeability, and mineralogy, are similar. Core samples are first saturated with the Montney oil using an accumulator, and then are placed in the Amott cells, and soaked in different brine samples. The experimental setup for spontaneous imbibition tests is described in our previous study (Habibi et al., 2016). The oil produced from the two similar cores is observed and collected over time until no more oil production is observed on the core surface. The experiment setup is shown in Figure 5.1.

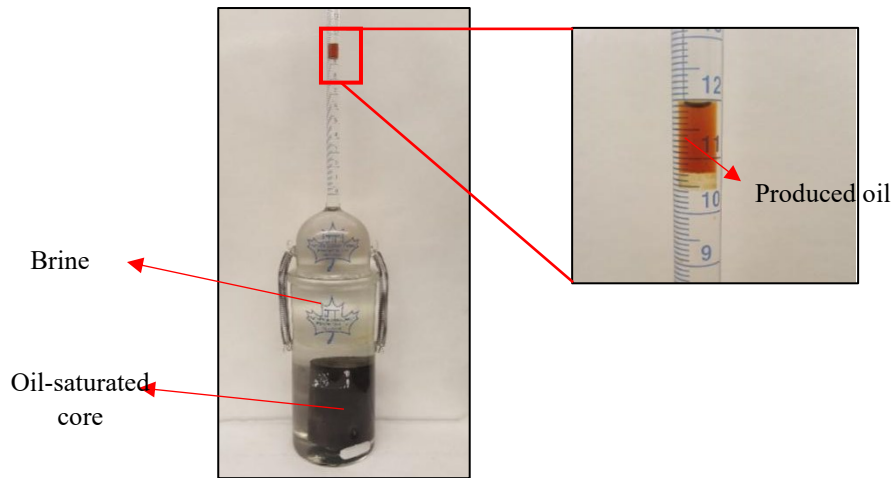


Figure 5.1 Amott cell used for soaking of oil-saturated core plugs in different soaking fluids.

5.3 Results and Discussion

5.3.1 Imbibition Oil Recovery Results. The CA results show that oil CA in the treated NaCl solution is higher than that in the untreated one. Here, we compare the imbibition oil recovery by treated brine, untreated brine, and untreated brine + oxidants to evaluate the effects of the EO process and added oxidants on imbibition oil recovery. We used NaCl solution only in these tests because NaCl ions are the most abundant ions in the FB. Cores 1 to 4, listed in Tables 4.1 and 4.2, are used for spontaneous imbibition tests since they have similar porosities, permeabilities, and mineralogy. All plugs are cut in half, and we assume that the half plugs have the same

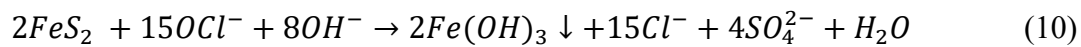
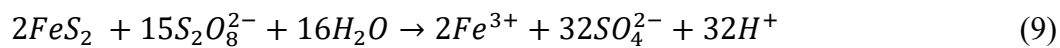
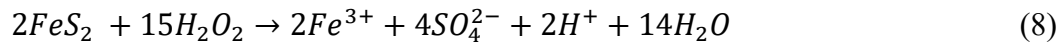
petrophysical properties. For cores 1 and 4, one of the half plugs is soaked in untreated brine, and the other half is immersed in treated brine to evaluate the effect of the EO treatment on imbibition oil recovery. For cores 2 and 3, one of the half plugs is soaked in untreated brine, and the other one is soaked in untreated brine + oxidants (NaOCl for core 2 and H₂O₂ for core 3). The effects of NaOCl and H₂O₂ on imbibition oil recovery are investigated here. The soaking time for each test is around 300 h, and the produced volume of oil can be observed on top of the Amott cell. Table 5.1 lists the values of produced oil (on top of the Amott cell) and the calculated oil recovery factor (RF) for Therefore, the enhancement of oil production by treated brine is not guaranteed although we observed that the rock is more water-wet in the treated NaCl solution than in the untreated one. We then compared the oil recovery by adding oxidants to study how NaOCl and H₂O₂ affect the imbibition oil recovery. Core 2 was used to study the effect of NaOCl, while core 3 was used to study the effect of H₂O₂. For core 2, the half plug in untreated NaCl with NaOCl produced 7.3% of oil, which is 2% less than the other half plug in untreated NaCl. This result suggests that the presence of NaOCl in the aqueous solutions may reduce oil production. Furthermore, for core 3, the oil recovery in untreated NaCl + H₂O₂ is about 32.2%, only 0.7% higher than the oil recovery in untreated NaCl, suggesting that H₂O₂ can slightly increase oil production. H₂O₂ can make the rock more water-wet based on our CA measurements, but it cannot significantly increase oil production.

Table 5.1 The produced oil and calculated oil recovery factor for each case.

Sample	Soaking Fluid	Initial Oil (cc)	Produced Oil (cc)	Oil RF (%initial oil in cores)
1	Untreated NaCl;	1.76	0.34	19.3%
	Treated NaCl	1.67	0.38	22.7%
2	Untreated NaCl;	1.08	0.1	9.3%
	Untreated NaCl +NaOCl	1.09	0.08	7.3%
3	Untreated NaCl;	1.27	0.4	31.5%
	Untreated NaCl +H ₂ O ₂	1.24	0.4	32.2%
4	Untreated NaCl;	1.80	0.4	22.2%
	Treated NaCl	1.86	0.32	17.2%

5.3.2 Precipitation in Spontaneous Imbibition Tests. We also observed precipitation on the rock surface in the spontaneous imbibition tests. Figure 5.2 shows the images of the produced oil droplets on the rock surface. These pictures were taken at the same soaking time. From the pictures, we found that reddish-brown precipitates form on the rock surface of cores 1, 2, and 4 as shown in panels (e, f, and g), respectively. Cores 1 and 4 were immersed in a treated NaCl solution, and core 2 was soaked in untreated NaCl + NaOCl solution. By comparing panels (f) and (g), we observed that the reddish-brown precipitates formed on core 2 in untreated NaCl + NaOCl but not on core 3 in untreated NaCl + H₂O₂, suggesting that the formation of precipitation is caused by NaOCl, not H₂O₂. Liang and Sheng (2020) also observed a large amount of reddish-brown precipitates forming on the rock sample treated with the NaOCl solution. They found that the reddish-brown precipitates are iron hydroxide (Fe(OH)₃), and the formation of Fe(OH)₃ is due to the oxidation of pyrite (FeS₂). The same observation was reported by Jew et al. (2017) In their study on Fe cycling in hydraulically fractured shales, they observed that a significant amount of

Fe²⁺ was released from pyrite in an acidic environment and then it was oxidized to Fe³⁺ by dissolved oxygen. As the solution pH increased to 3.25, ferrihydrite started to precipitate in the shale matrix, and it eventually transformed to either goethite (at pH 2.0) or hematite (pH > 6.5) as the experimental time was increased. The reaction between pyrite and oxidants can be generally expressed by:



Pyrite in the rock sample can be easily oxidized to Fe³⁺ and SO₄²⁺ by NaOCl, H₂O₂, or Na₂S₂O₈. The OH⁻ ions released from NaOCl (eq 7) cause rapid and effective formation of Fe(OH)₃ (eq 10). Fe(OH)₃ may also form when adding H₂O₂ and Na₂S₂O₄ to the aqueous solution. However, the amount of Fe(OH)₃ precipitates should be significantly less due to the limited amount of OH⁻ (eqs 8 and 9). In our imbibition tests, the precipitates observed on the half plugs of cores 1 and 4 in the treated NaCl solution may be Fe(OH)₃. However, the amount of precipitation on core 1 is significantly less than that on core 4. The results showed that core 1 in treated NaCl produced more oil than that in untreated case, while core 4 in untreated NaCl produced more oil than that in the treated case. Therefore, we hypothesize that formation of a large amount of precipitates on core 4 can be the reason for low oil recovery. The imbibition tests on cores 2 and 3 also support this conjecture. For the half plug of core 2 soaked in untreated NaCl + NaOCl, some precipitates (possibly Fe(OH)₃) are observed on the rock surface. This may explain why the oil production from this half core is less than that from the other half in untreated NaCl. No precipitates were observed on the rock surface for the half plug of core 3 soaked in untreated NaCl solution with H₂O₂ that may explain why both half plugs have similar production. Overall, our CA results

suggest that EO treatment can make the rock more water-wet, but the spontaneous tests suggest that improvement in oil recovery is not guaranteed. We observed that oil recovery for core 1 and core 3 is slightly higher in the treated brine. However, oil recovery was not enhanced for core 2 and core 4 in the treated brine, and a significant amount of reddish-brown precipitates can be observed on the rock surface. Therefore, we conclude that the treated brine can slightly improve oil recovery, but the dissolution and reprecipitation of minerals may block the pores near the surface and reduce the recovery efficiency.

Core 1



(a)

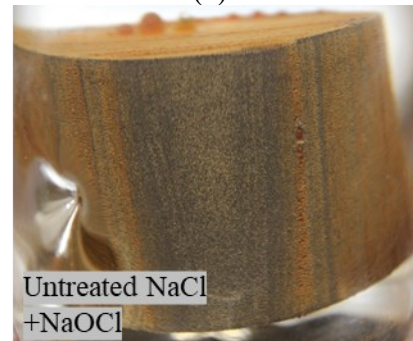


(e)

Core 2

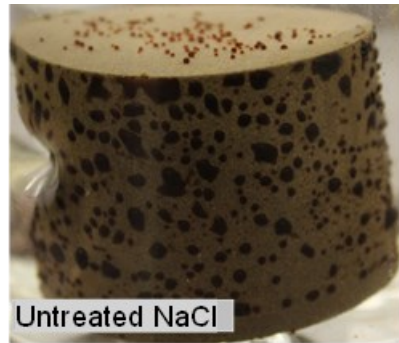


(b)

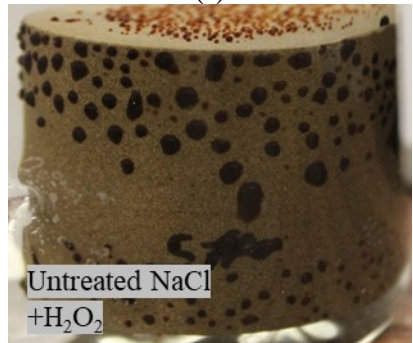


(f)

Core 3



(c)



(g)

Core 4



(d)



(h)

Table 5.2 Picture of rock samples used in the spontaneous imbibition tests using 90,000 ppm (a-d) untreated NaCl; (e) treated NaCl; (f) untreated NaCl + NaOCl; (g) untreated NaCl+ H₂O₂ (h) treated NaCl.

Chapter 6 Literature Review on Fracturing Fluid and Research Gap

6.1 Review on Hydraulic fracturing and Friction Reducer

Oil extraction from low permeability reservoir often requires hydraulic fracturing operation to increase the conductivity of the formation rock. By fracturing, new channels and connections between existing pores or channels allow the hydrocarbon to flow and produce at economical rates (Guo et al., 2022). Among many breaking strategies for fracturing, slickwater fracturing has been shown to be an effective technique to create and expand the cracks in the tight rock and improve hydrocarbon recovery (Sun et al., 2014).

Friction reducer (FR) is one of the critical chemical additives used to prepare the slickwater before the hydraulic fracturing process. Because of high displacement during the fracturing, fracturing fluid usually suffers huge energy loss from interaction among pipeline surface, proppants and fluid (Yang et al., 2019). To compensate for those energy losses, the surface operation must increase its wellhead pressure to ensure enough energy transfer to the downhole. However, high wellbore pressure may lead to many safety issues during fracturing operations (Sun et al., 2013). FR provides a solution for reducing energy loss without too much wellhead pressure increment. Adding a small amount of FR to the fluid allows the fluid to move in the wellbore at faster rates but using less horsepower (Sun et al., 2011). Because of the fluid's relatively high viscosity and viscoelasticity, the operations can maintain the fluid in lamination and carry the proppants to the downhole without too much energy loss. (Guo et al., 2022). In return, surface operation requires less extra energy to compensate for the energy loss (Sun et al., 2011).

The most commonly used FR are Xanthan, Guar, polyacrylamide (PAM), and hydrolyzed polyacrylamide (HPAM) (Ba Geri et al., 2019). Natural friction reducers, such as guar and xanthan, are widely used in conventional reservoir fracturing. Using natural FR have the following

advantages: 1) they are relatively cheap, 2) they have good solubility, 3) they are environmentally friendly and biodegradable (Yang et al., 2019), and 4) they are less sensitive to mechanical degradation (Al-Hajri et al., 2022). However, the drag reduction rate of those polymers is relatively low, ranging from 30% to 65%, depending on the concentration of those FRs (Wyatt et al., 2011). PAM and HPAM are long-chain polymers with linear structures. They have high water solubility, good thermal stability and an effective drag reduction rate (Yang et al., 2019). PAM is an elastic polymer formed from a single monomer of acrylamide, while HPAM is an elastic polymer formed from the monomers of acrylamide and acrylic acid (Figure 6.1). The drag reduction for PAM and HPAM can easily reach 75% at a concentration of around 0.1 wt % (Escudier & Smith, 2001; Wang et al., 2016). Due to an additional hydrophobic group (acrylic acid) in HPAM molecules, the solubility of the polymer and intermolecular association between polymers are typically stronger than the solubility and association of PAM molecules (Taylor & Nasr-El-Din, 2007). Therefore, HPAM is advantageously employed for proppant transportation (Yang et al., 2019).

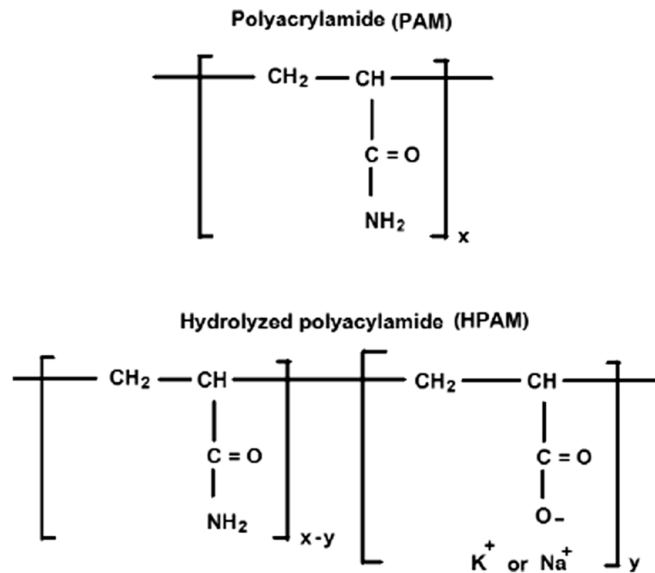


Figure 6.1 Structure of PAM and HPAM (Gbadamosi et al., 2019)

However, the major problems for slickwater fracturing are consuming a large amount of fresh water and producing a large amount of wastewater. According to Arthur et al. (2009), successfully developing one horizontal well for unconventional plays requires between 3 million to 4 million gallons of water. Some of the companies may struggle with finding water supplies to meet the development needs, especially in areas that lack freshwater resources. Once the fractures have been created, releasing the wellbore pressure will lead to fracturing fluid combined with formation brine flow back through the well casing to the wellhead. This is referred to as flowback water. According to Yap et al. (2016), up to 60% of fracturing fluid can flow to the surface within 2-4 weeks after the fracturing treatment. Furthermore, formation water will continue to be generated and flow to the surface with hydrocarbon during the hydrocarbon production (Shih et al., 2015). Both flowback water and formation water are considered oil field waste and need to be transported and treated before injection into the disposal wells (Igunnu & Chen, 2014).

6.2 Research Gap

Considering the recent increase in water-disposal costs and environmental concerns, the industry is encouraged to reuse the produced water after hydraulic fracturing operations. However, the complex nature of the flowback or produced brine makes reusing of the produced water challenging.

Some ions such as Ca^{2+} , Mg^{2+} , Fe^{3+} above specific salinity may cause the curling and agglomeration of FR and reduce their functionality, leading to an inefficient proppant transport (Paktinat et al., 2011; Muller et al., 1979). This section presents a series of experiments to investigate the effects of ion type and concentration on the performance of friction reducers such as HPAM at 1 mg/ml in produced water from Montney formations. The objectives are to 1) identify

the problematic ions that may react with HPAM, 2) determine their threshold concentration above which HPAM curling may occur. The results can be applied to designing a cost-effective procedure for treating produced water while maintaining the stability of friction reducers.

Chapter 7 Problems with Reuse of Untreated Brine for Hydraulic Fracturing

In this section, we conduct particle size distribution, dynamic (shear) viscosity, and viscoelastic properties measurements after adding HPAM to synthetic Montney-produced brine and deionized (DI) water. Here, we compare those properties to investigate and predict the outcome of reusing untreated produced brine for hydraulic fracturing operations.

7.1 Material

7.1.1 Friction Reducer. We use HPAM as FR in our experiments. The HPAM is purchased from SNF Floerger Company, it has an average molecular weight of about 8 million g/mol, and the degree of hydrolysis is about 25-30%. To perform this study, a HPAM concentration of 1 mg/ml was chosen.

7.1.2 Fluid Sample. The aqueous solutions used for experiments are DI water and synthetic FB with TDS of 135,000 ppm, and its composition is presented in Table 3.1. The dominant ions in FB are Na^+ , Ca^{2+} , and Cl^- .

7.2 Methodology

7.2.1 Sample Preparation

HPAM solutions are prepared using the following steps:

- Both DI water and prepared synthetic brine were first stirred at 400 rpm overnight to remove the air bubbles.
- The amount of HPAM was first calculated based on the volume of the DI water and synthetic brine. Then, we gradually added HAPM to the stirring DI water and synthetic brine until it reached 1 mg/ml.

- After adding the HPAM, the solution was stirred at 100 rpm for 3 hours until the HPAM powder fully dissolved.
- The HPAM solution was then removed from stirring and allowed to stand overnight to reach the maximum degree of hydrolysis.

7.2.2 Density and Surface Tension Measurements

The density and surface tension of the HPAM solution was measured using an Attension Sigma 700 tensiometer (Biolin Scientific, Sweden). (as shown in Figure 3.2a) Three density and surface tension readings were taken and reported in an average value for every test fluid. The objective of this measurement is to investigate the influence of the HPAM on surface tension.

7.2.3 Particle Size Distribution Measurements

The hydrodynamic size of the HPAM in the aqueous solutions was measured using a Malvern Zetasizer Nano zs (as shown in Figure 7.1) at room temperature and atmospheric pressure based on the dynamic light scattering (DLS) method. The hydrodynamic size for each sample was measured three times to ensure repeatability.



Figure 7.1 Zetasizer Nano zs for particle size analysis

7.2.3 Dynamic Viscosity and Viscoelasticity Measurement

The dynamic viscosity and viscoelasticity of each HPAM solution were determined using Anton Paar Rheometer MCR 302 (Figure 7.2). During the measurement, the Viscosity and shear stress profile with respect to shear rate, and viscoelastic components storage modulus (G') and loss modulus (G'') with respect to angular frequency can be obtained to evaluate the shear resistance and energy loss of each HPAM solution. All measurements were repeated three times to ensure repeatability.



Figure 7.2 Anton Paar Rheometer MCR 302 for measuring dynamic viscosity and shear stress at different shear rate, and viscoelastic components G' (storage modulus) and G'' (loss modulus) at different angular frequency.

7.3 Results and Discussion

7.3.1 Density and Surface Tension Measurement

Table 7.1 shows the measured density and surface tension values of HPAM solutions at room temperature (25 °C). The density of HPAM in DI water and FB are 0.996 g/cm³ and 1.113 g/cm³, respectively. Because the concentration of the HPAM in DI water and in FB is 1 mg/ml, the density difference between HPAM in DI water and FB mainly depends on the density of the aqueous

solution. The surface tension of the DI water with HPAM is about 63.97 mN/m, which is higher than the surface tension of HPAM in FB (41.41 mN/m).

Table 7.1 Measured value of density and surface tension of HPAM solutions

	Density (g/cm ³)	Surface Tension (ST) (mN/m)
HPAM in DI Water	0.996	63.97±0.28
HPAM in FB	1.113	41.41±0.42

7.3.2 Shear Viscosity and Shear Stress Measurements

According to the results from other papers, all slickwater used for hydraulic fracturing operations should exhibit a non-Newtonian fluid with shear-thinning behavior, and the relationship follows the power law, which is shown as: ((Malhotra & Sharma, 2012; Sun et al., 2014; Wei et al., 2022)

$$\mu_a = K\gamma^n$$

Where μ_a is the dynamic shear viscosity; γ is the shear rate. The K parameter is the power-law consistency factor that determines the yield stress of fluid, the higher value of the K represents the more viscous fluid. Also, this parameter can be significantly affected by the temperature (Ba Geri et al., 2019). The n parameter is the flow behavior index which determines rheological properties. The flow behavior of the fluid is Newtonian when $n = 1$, and non-Newtonian when $n \neq 1$. It is also worth mentioning that the value of $n < 1$ indicates the shear-thinning behavior, and the value of $n > 1$ implies the shear-thickening behavior (Biheri & Imqam, 2021).

Figure 7.3a shows the shear stress vs shear rate plot obtained from dynamic viscosity measurements for two of the experimental fluid (1mg/ml HPAM in DI water, and 1mg/ml HPAM in FB), while Figure 7.3b shows the shear viscosity vs shear rate plot obtained from the same experiment. Table 7.2 lists the K parameter, n parameter, and R² value for HPAM solutions. As listed in the Table, the K parameter, n parameter and R² value for HPAM in DI water are 0.947 Pa·sⁿ, 0.216, and 0.949, respectively, indicating that the flow behavior is a typical power-law non-

Newtonian fluid. The K, and n parameters for HPAM in FB are 0.163 Pa·Sⁿ, and 0.037, respectively. The n parameter suggests that the flow behavior of HPAM in FB is also a non-Newtonian fluid with shear thinning behavior. However, the HPAM in FB has a small R² value (0.011), indicating a significant variation in the shear stress that is explained by the regression. Small K and n parameters suggest that the viscosity of HPAM in FB is low, and it can be more affected by shear rate increment than HPAM in DI water, and the suspension effect for proppant transportation may be less effective (Ba Geri et al., 2019; Ba Geri, Imqam, et al., 2019). Both small K, n parameter and R² value are probably due to the HPAM agglomeration in the FB, which HPAM molecules are not stable in FB, and the agglomeration may negatively impact the viscosity measurement results. (As shown in Figure 7.4).

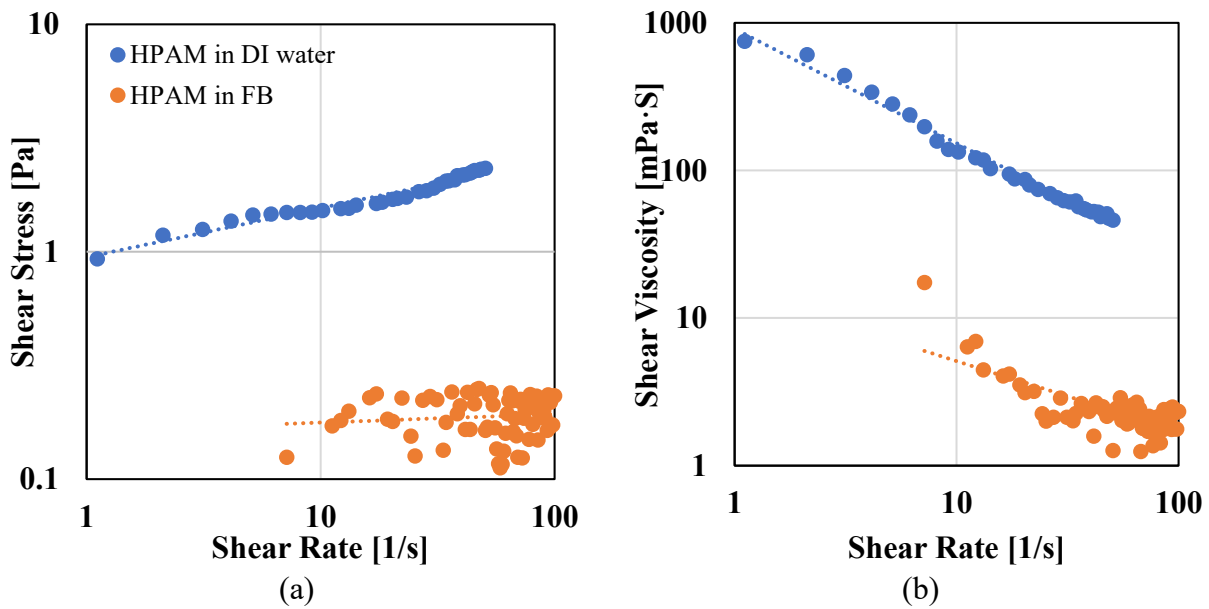


Figure 7.3 The variation of a) shear stress and b) shear viscosity with shear rate for HPAM in DI water and FB

Table 7.2 Power-law parameter, including power-law consistency factor (K) and flow behavior index (n), and R-squared value for HPAM solution

	K(Pa·S ⁿ)	n	R ²
HPAM in DI Water	0.947	0.216	0.949
HPAM in FB	0.163	0.037	0.011

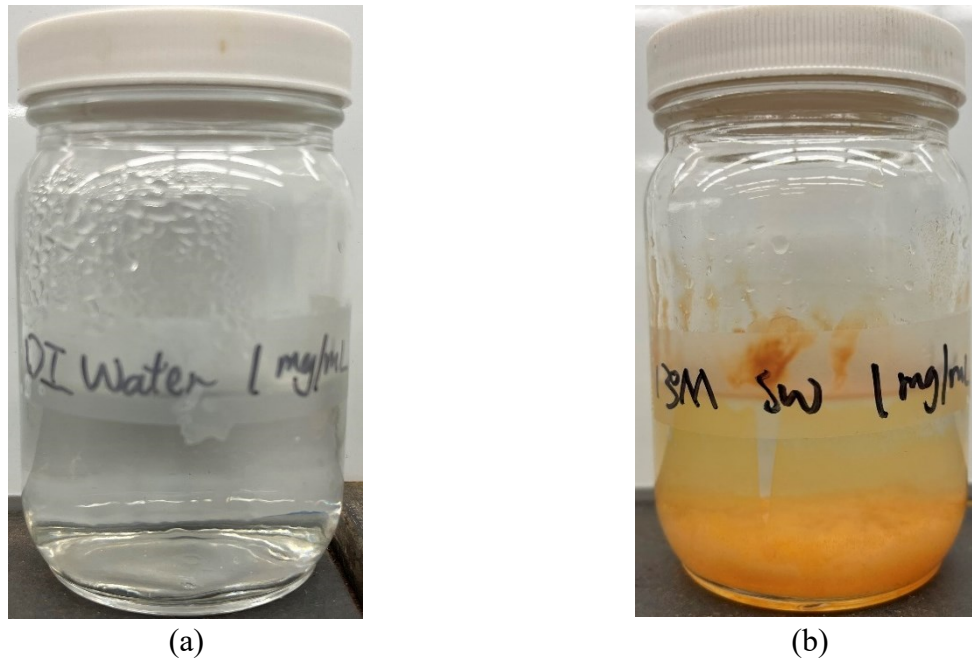


Figure 7.4 The picture of prepared HPAM solutions using a) DI water, b) FB

7.3.3 Particle Size Distribution of HPAM

Here, we measured the hydrodynamic size of HPAM in the solutions. This part aims to determine the hydrodynamic size difference of HPAM particles when we use different aqueous solutions to prepare the slickwater. Dynamic light scattering (DLS) was used to analyze the hydrodynamic size of HPAM in DI water and FB

Figure 7.5 shows the PSD profile on HPAM solutions. The x-axis represents the particle diameter of the polymer in the HPAM solution, while the y-axis represents the intensity in percentage. The average value for each peak and its standard deviation are summarized in Table 7.3

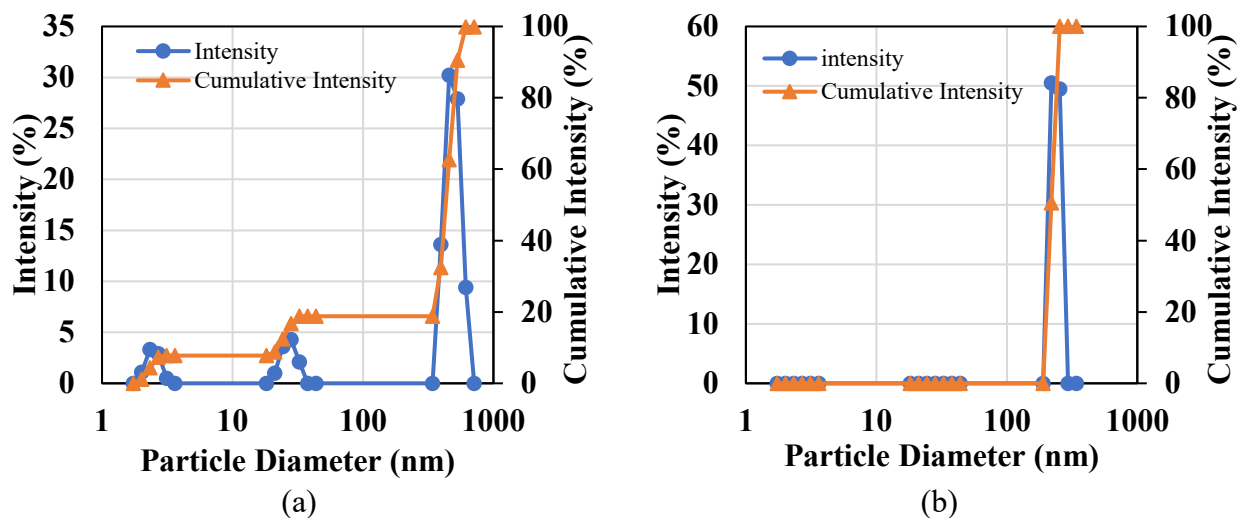


Figure 7.5 The hydrodynamic size of the HPAM molecules in a) DI water, b) FB

Table 7.3 The average hydrodynamic size of the HPAM and its standard deviation

	Peak 1		Peak 2		Peak 3	
	Size (nm)	St Dev (nm)	Size (nm)	St Dev (nm)	Size (nm)	St Dev (nm)
HPAM in DI Water	491.3	65.09	27.13	3.50	2.472	0.2923
HPAM in FB	237.4	17.4	N/A	N/A	N/A	N/A

From the Figure and Table, we observed three hydrodynamic sizes for HPAM in DI water and one hydrodynamic size for HPAM in FB. More than 80 % of HAPM particles in DI water have an average size of about 491.3 nm, while 100% of HPAM in FB have an average size of about 237.4 nm, which is smaller than the average hydrodynamic size of HPAM in DI water. Wang et al. (2022) measured the hydrodynamic size distribution of polymer in salts solution with salinity ranging from 0 to 60,000 ppm. They found that the polymer in DI water has the largest hydrodynamic size, and the size decreases as the salinity increase. They explained that the shrink in hydrodynamic size with increase in salinity is due to the electrostatic screening effect caused by salt ions, which inorganic salts is adsorbed on the surface of the polymer main chain to shield the carboxyl groups from electrostatic repulsion. Silva et al. (2018) measured the hydrodynamic size of HPAM in DI water, 500 ppm, 38,000 ppm NaCl solutions. They found that a reduction of hydrodynamic size of

HPAM particles with rising salinity. They also attributed to the shielding of the negative charges of the carboxylate groups of the polyacrylamide by the cations present in the dispersion medium.

7.3.4 Viscoelastic Properties Measurements

Oscillatory tests were carried out on each test fluid to determine each fluid's viscoelastic properties and relaxation time. Figure 7.6 represents the oscillation test results for two experimental fluids (HPAM in DI water and HPAM in FB). In the tests, we measured the storage and loss modulus to determine the viscoelasticity, where G' is the storage modulus, representing the elastic response, and G'' is the loss modulus, representing the viscous response. Viscoelastic properties of fracturing fluid significantly contribute to the efficiency of proppant transport inside fractures (Biheri & Imqam, 2021b). In general, when storage modulus G' is less than loss modulus G'' , the intermolecular association between polymer is weak, and the effective structure to suspend proppant does not form. Therefore, the fluid behaves more like a liquid. In contrast, when G' is more than G'' , the degree of intermolecular association between polymers is strong, and the fluid behaves more like a solid (Zhao et al., 2018; Wang et al., 2016). The inverse of the crossover point, where G' is equal to G'' , can be referred to as the relaxation time of the polymer network. The longer fluid relaxation time suggests a better proppant suspension ability (Biheri & Imqam, 2021b).

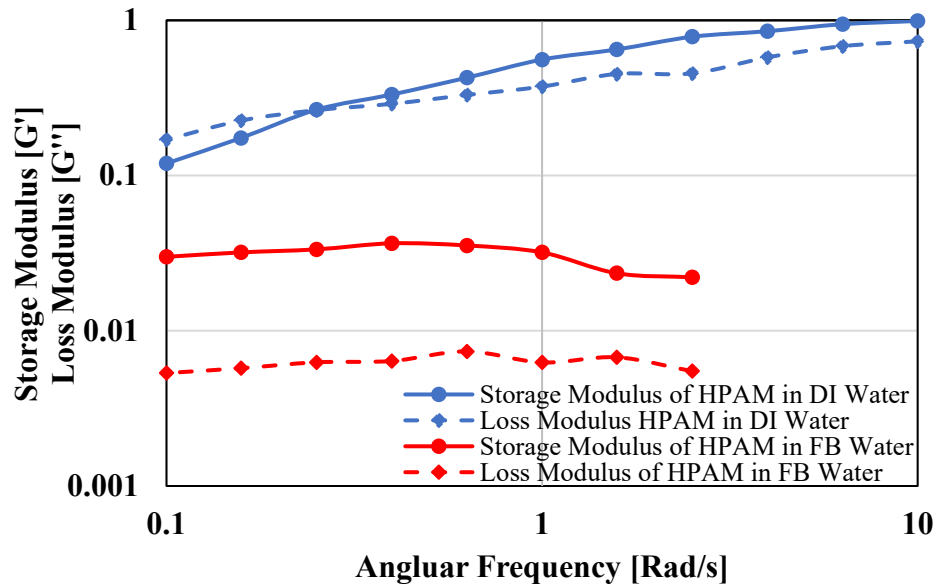


Figure 7.6 Viscoelastic properties at room temperature: storage and loss modulus of HPAM in DI water and FB with respect of angular frequency

From Figure 7.6, we observed that G' is less than the G'' for HPAM in DI water at the angular frequency <0.25 rad/s. The G' and G'' profiles cross at the angular frequency of 0.25 rad/s, indicating that the relaxation time is 4 s. G' is higher than G'' when the frequency is above 0.25 rad/s, which shows viscoelastic behavior with significant elasticity at high frequencies. However, the G' of HPAM in FB is always approximately six times larger than G'' in the entire measured range, indicating a significant entanglement between the HPAM molecules, and the elasticity of the solution leads the properties. No crossover points for HPAM in FB indicate that the energy stored elastically in the HPAM molecules cannot efficiently transfer to the viscous energy. The above analysis indicates that the HPAM particles in the FB has undergone a considerable conformation change due to the stimulation of salt ions in the solution. The backbone of HPAM molecules has been curled due to the electrostatic screening effect caused by salt ions (Wang et al., 2022). This can also be confirmed through Figure 7.4, in which HPAM aggregate and precipitate in the FB.

To conclude, HPAM in the FB has a much lower viscosity profile along all the shear rate ranges compared to the HPAM in DI water, indicating that slickwater prepared with FB is easier to generate turbulent flow than with DI water. Hydrodynamic size of HPAM in DI water and FB indicate that the salt ions in the FB can cause the reduction of size HPAM. Viscoelastic properties measurements results show that G' is well above G'' for HPAM in FB in the frequency range, indicating a considerable curling of HPAM in the FB.

Chapter 8 The Effect of Cations and its Salinity on Shear Viscosity

In this chapter, we add HPAM to the different aqueous solutions, including NaCl, CaCl₂, MgCl₂ and FeSO₄, with various salt concentrations to identify the problematic ions and their threshold concentration. We evaluate the compatibility between HPAM and different salts through the shear viscosity measurement.

8.1 Material

8.1.1 Friction Reducer. We use HPAM for our experiments. Information about HAPM can be found in Chapter 7. The HPAM concentration used in this study is about 1 mg/ml.

8.1.2 Fluid Samples. In order to evaluate the effect of the type of salt on the shear viscosity of the HPAM solution, each salt of a synthetic formation water composition was individually evaluated. The salts used to prepare the different brine solutions were sodium chloride (NaCl), calcium chloride dihydrate (CaCl₂·2H₂O), magnesium chloride (MgCl₂), and Ferrous sulfate (FeSO₄·7H₂O). The total dissolved solid (TDS) of the original brine is 135,000 ppm, and its composition is present in Table 3.1. To understand the role of each type of cation on the performance of slickwater, we conduct a sensitivity analysis to determine the threshold concentration of each cation through dynamic viscosity. We selected three different concentrations, including 100,000 ppm, 10,000 ppm and 1,000 ppm for NaCl, CaCl₂ and MgCl₂ aqueous solution, and 10,000 ppm, 1,000 ppm and 100 ppm for FeSO₄ aqueous solution. The slickwaters were prepared by mixing HPAM with aqueous solutions for approximately 3 hours, then hydrated overnight to ensure it was fully hydrated.

8.2 Methodology

8.2.1 Sample Preparation. HPAM solutions are prepared by following the steps in Chapter 7.

8.2.2 Dynamic Viscosity Measurements. The dynamic viscosity of HPAM solutions was measured using Brookfield cone/plate Viscometer (as shown in Figure 3.2b). All tests were performed at room temperature and pressure. Each sample's dynamic viscosity and shear stress were measured by setting the shear rate from 0.1 to 200 rpm to obtain the dynamic viscosity profile. The power-law parameter, including the power-law K parameter, n parameter, and R^2 value of HPAM solutions, were determined using the linear trendline function of Microsoft excel.

8.3 Results and Discussions

8.3.1 Density and Surface Tension Measurements

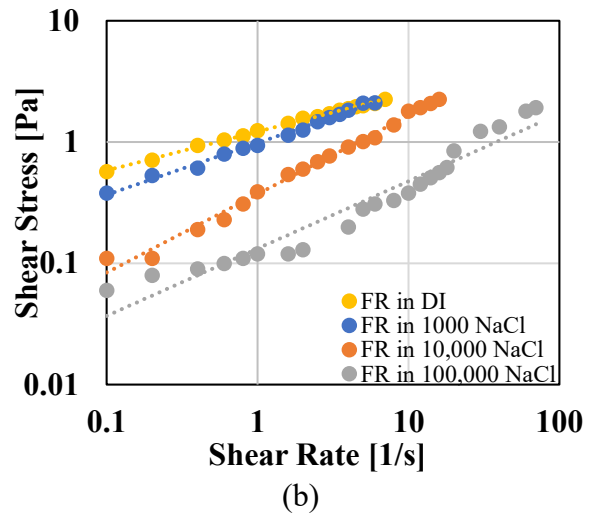
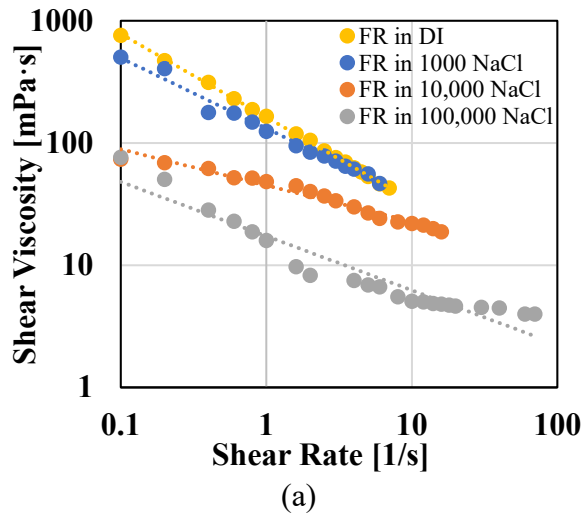
Table 8.1 lists the measured density and surface tension of HPAM in NaCl, CaCl₂, MgCl₂ and FeSO₄ solution with various concentrations at room temperature (25 °C). Because the concentration of the HPAM in all aqueous solutions is 1 mg/ml, the density difference between each aqueous solution mainly depends on the density of the aqueous solution. From the table, we also observed that the surface tension of HPAM solutions decreases with salts concentration. We also observed less surface tension in the high valence cation solution to compare the surface tension of different aqueous solutions with the same salinity. For example, the surface tension of HPAM in MgCl₂ and CaCl₂ solution are lower than that of HPAM in NaCl solution with similar salinity. HPAM in FeSO₄ has lower surface tension than HAPM in MgCl₂ and CaCl₂ solution. This is because that Fe²⁺ can be easily oxidized to Fe³⁺ at ambient temperature and pressure. The surface tension reduction trend observed in table 8.1 is due to the presence of salts in the solution rather than the addition of HAPM. When adding salts to the water, positive and negative ions can interact with the negative and positive ends of the water-molecule-electric-dipole. As a result, the interaction between water molecules is lessened, and the surface tension is correspondingly lessened.

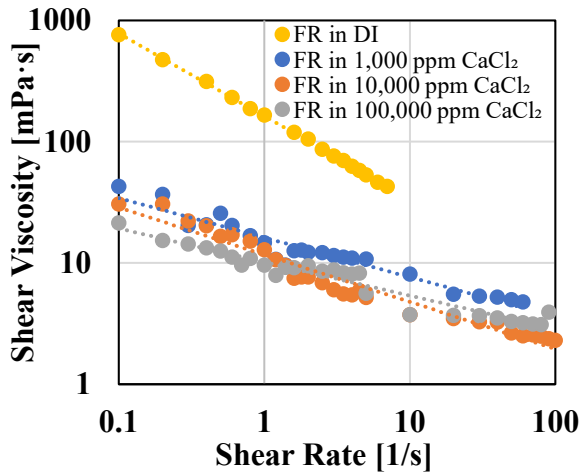
Table 8.1 Measured value of density and surface tension of HPAM in different aqueous solutions

	Density (g/cm ³)	Surface Tension (mN/m)
HPAM in DI water	0.996	63.97±0.28
HPAM in 1,000 NaCl solution	1.003	61.42±0.21
HPAM in 10,000 NaCl solution	1.006	56.5±0.18
HPAM in 100,000 NaCl solution	1.071	46.65±0.19
HPAM in 1,000 CaCl ₂ solution	1.005	59.91±0.52
HPAM in 10,000 CaCl ₂ solution	1.01	50.38±0.21
HPAM in 100,000 CaCl ₂ solution	1.074	40.77±0.17
HPAM in 1,000 MgCl ₂ solution	1.003	57.93±0.13
HPAM in 10,000 MgCl ₂ solution	1.006	52.11±0.16
HPAM in 100,000 MgCl ₂ solution	1.077	41.86±0.53
HPAM in 100 FeSO ₄ solution	0.998	55.94±0.13
HPAM in 1,000 FeSO ₄ solution	1.006	51.25±0.09
HPAM in 10,000 FeSO ₄ solution	1.013	49.58±0.07

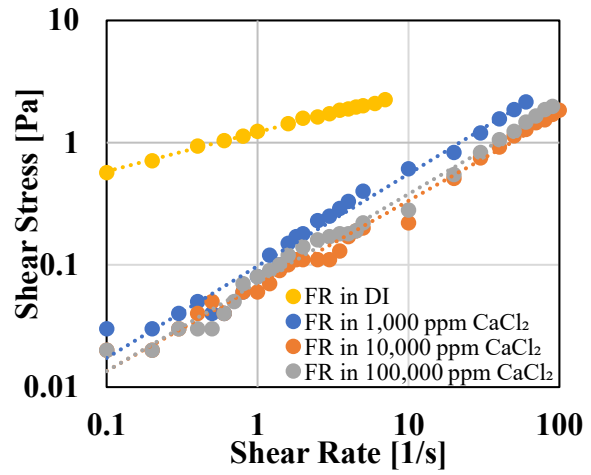
8.3.2 Shear Viscosity Measurements

Here, we measured and compared the shear viscosity of the HPAM in different aqueous solutions to investigate the effect of cations and salinity through dynamic viscosity.

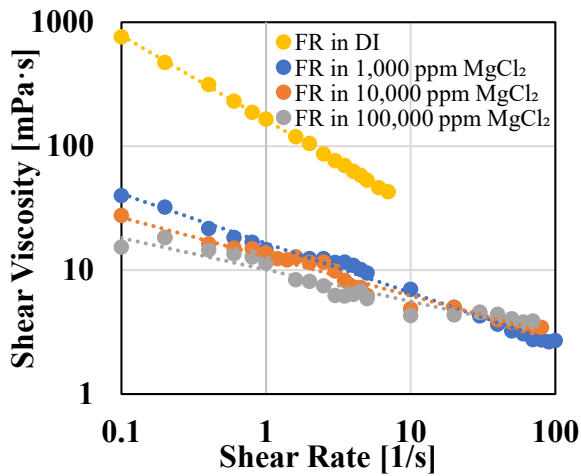




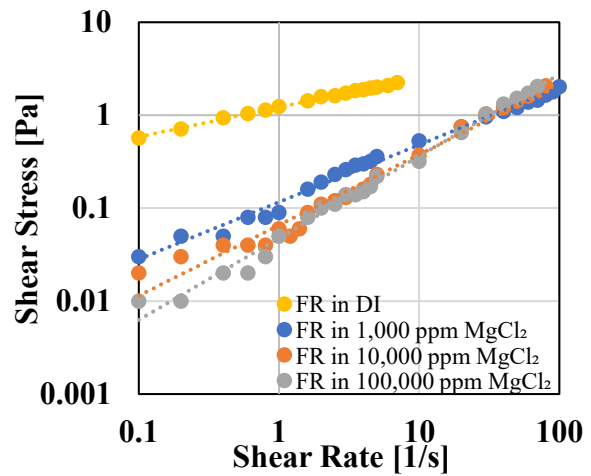
(c)



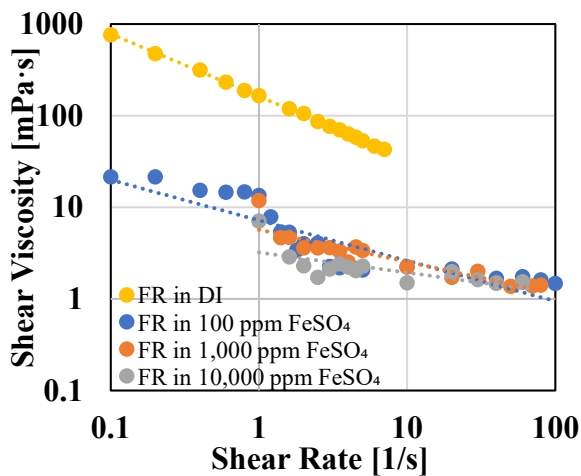
(d)



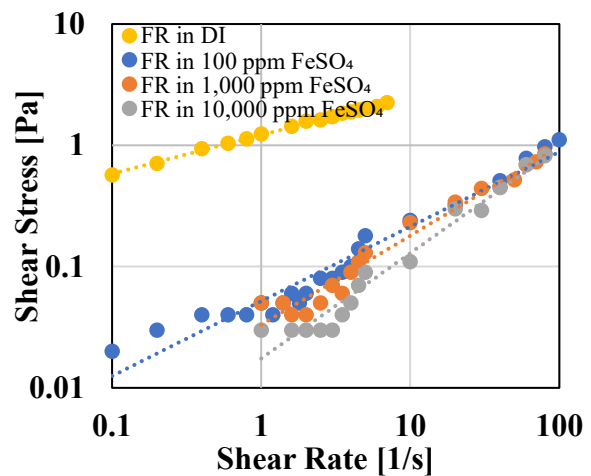
(e)



(f)



(g)



(h)

Figure 8.1 The variation of shear viscosity and shear stress with shear rate for HPAM in a,b) NaCl, c,d) CaCl₂, e,f) MgCl₂, g,h) FeSO₄ aqueous solutions

Table 8.2 Power-law parameter, including power-law consistency factor (K) and flow behavior index (n), and R-squared values for HPAM in different aqueous solutions

	K (Pa·s ⁿ)	n	R ²
HPAM in DI water	1.217	0.319	0.998
HPAM in 1,000 NaCl solution	0.984	0.428	0.993
HPAM in 10,000 NaCl solution	0.372	0.647	0.990
HPAM in 100,000 NaCl solution	0.132	0.554	0.938
HPAM in 1,000 CaCl ₂ solution	0.098	0.775	0.974
HPAM in 10,000 CaCl ₂ solution	0.072	0.725	0.974
HPAM in 100,000 CaCl ₂ solution	0.067	0.697	0.988
HPAM in 1,000 MgCl ₂ solution	0.116	0.617	0.991
HPAM in 10,000 MgCl ₂ solution	0.066	0.759	0.976
HPAM in 100,000 MgCl ₂ solution	0.048	0.881	0.990
HPAM in 100 FeSO ₄ solution	0.052	0.616	0.961
HPAM in 1,000 FeSO ₄ solution	0.033	0.735	0.969
HPAM in 10,000 FeSO ₄ solution	0.017	0.869	0.961

It can be seen from the flow curve presented in Figure 8.1, that the addition of any salt negatively affects the dynamic viscosity of the fluid with no salt content. The K parameters, n parameters and R² values for the flow curves are presented in Table 8.2. For all the investigated HPAM solutions, the power law model provides a good fit to the data all over the range of shear rates used because of the large R² values.

8.3.3 Impact of Salinity on Dynamic Viscosity and Shear Stress

HPAM in DI water has the most significant K parameter, indicating the most viscous fluid in our study. When NaCl concentration increases from 0 to 1,000 ppm, the K parameter is slightly reduced from 1.217 to 0.984 Pa·sⁿ, indicating that the addition of NaCl negatively affects the dynamic viscosity of the fluid. As the NaCl concentration increases to 10,000 ppm and 100,000 ppm, the K parameters are correspondingly reduced to 0.372 and 0.132 Pa·sⁿ, respectively. Similar observations can be found in CaCl₂, MgCl₂ and FeSO₄ solutions, where the most considerable K parameters are always observed in the lowest salt concentration. However, the reduction of the K parameter in CaCl₂, and MgCl₂ solutions is not as significant as in NaCl solutions. Moreover, more

significant n parameters of the HPAM solutions are observed in NaCl, CaCl₂, MgCl₂ and FeSO₄ solutions than in DI water, suggesting that the viscosity of HPAM in salt water can be less affected by the shear rate increment. However, a larger n value for HPAM in salt water does not mean that using salt water is better than using DI water to prepare the slickwater. This is because HPAM in DI water has the largest dynamic viscosity at the low shear rate, which can deal with more shear rate increment than the HPAM in salt water.

8.3.4 Impact of Cation Valence on Dynamic Viscosity and Shear Stress

High-valence cations have a strong influence on the dynamic viscosity of HPAM solutions. From Figure 8.1 ab, HPAM in 1,000 ppm NaCl solution has slightly lower shear stress and dynamic viscosity profiles than the HPAM in DI water. However, HPAM in 1,000 ppm CaCl₂ and MgCl₂ have significantly lower shear stress and dynamic viscosity profiles than the HPAM in DI water (which can also be confirmed through K and n parameters). This suggests that HPAM can resist low levels of monovalent salts such as NaCl, but cannot resist low levels of divalent cations such as calcium and magnesium. As the concentration of salts increases to 10,000 ppm, and 100,000 ppm, a significant reduction in the K parameter are found in NaCl, CaCl₂ and MgCl₂ solutions, suggesting a loss in performance of HPAM with the presence of a high concentration of monovalent cations and divalent cations. The reason can be explained that the divalent ions (Ca²⁺ or Mg²⁺) and high concentration of monovalent cations are tightly bound to anions along the polymer chain due to the higher charge, causing the polymer chain to curl to its minimum size (Paktinat et al., 2011a).

8.3.5 Impact of Iron Ions on the Stability of the HPAM Solution

As seen in Figure 8.1 and Table 8.2, the presence of iron ions in the solution significantly reduces dynamic viscosity and shear stress more than calcium and magnesium ions. Even a 100 ppm FeSO₄

solution can cause the HPAM loss in performance, referred to as $0.052 \text{ Pa}\cdot\text{s}^n$ for the K parameter of HPAM in a 100 ppm FeSO_4 solution. This is because ferrous ions (Fe^{2+}) can be easily oxidized to ferric ions (Fe^{3+}) at room temperature and pressure, and ferric ions can make stretching the HPAM molecular more difficult than divalent ions reducing the effective viscosity. Further increase in iron ions concentration to 1,000 and 10,000 ppm will not cause a significant loss in dynamic viscosity. However, HPAM molecules are not stable at high levels of iron ion concentration, such as 1,000 and 10,000 ppm. Figure 8.2 shows the stability of HPAM in different aqueous solutions. As can be seen from Figure 8.2abc, there is no precipitation of HPAM in the NaCl , CaCl_2 and MgCl_2 solutions despite the concentration of salts as high as 100,000 ppm, indicating that HPAM is stable in those solutions. The HPAM molecules are also stable in 100 ppm FeSO_4 solution as there is no precipitate, as shown in Figure 8.2c. Further increasing the concentration of FeSO_4 to 1,000 ppm can cause the dissolved HPAM molecules to flocculate and precipitate at the bottom of the solution (as shown in Figure 8.2d). We also observed that HPAM powder had difficulty dissolving and hydrolyzing in 10,000 ppm FeSO_4 solution, as seen from the large particles in Figure 8.2e.

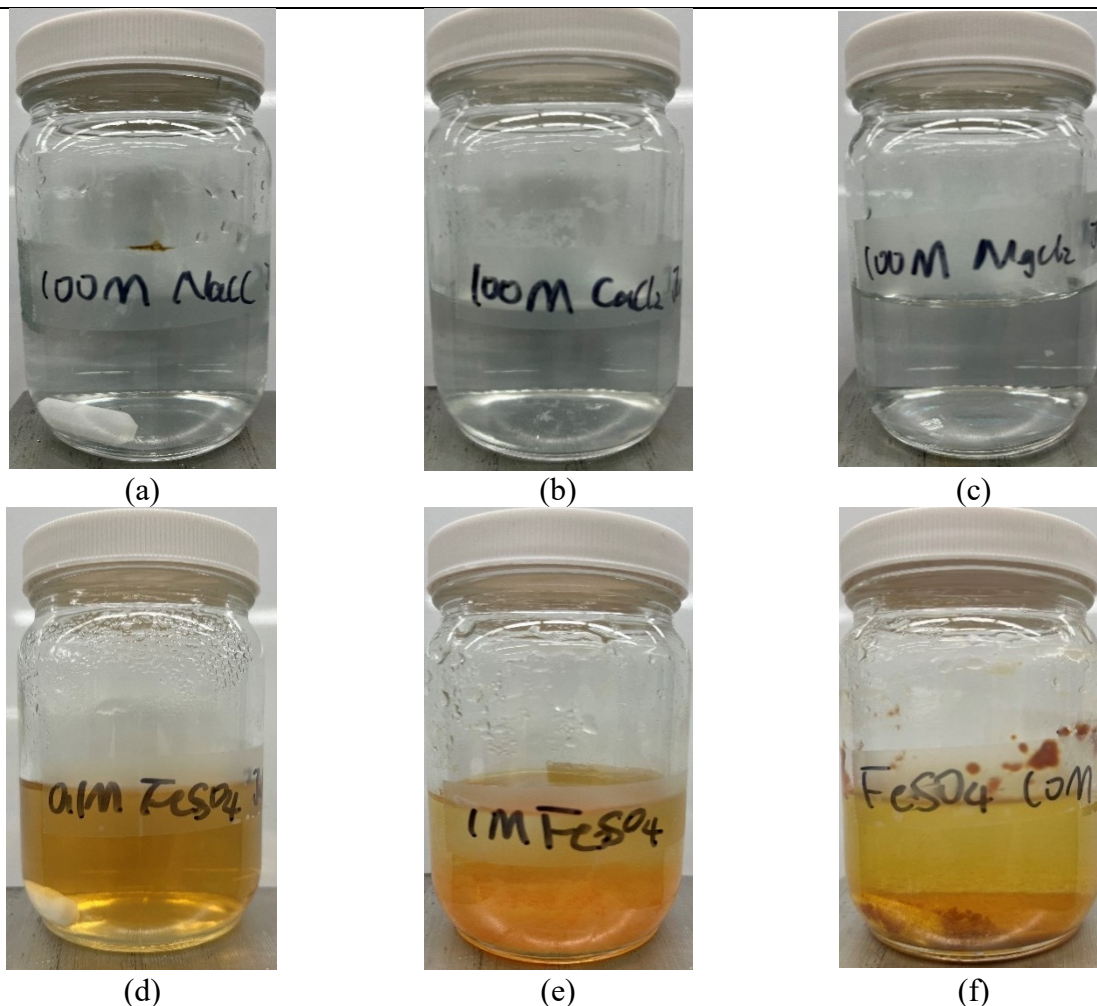


Figure 8.2 Picture of prepared HPAM solution for showing the stability of HPAM molecules in different aqueous solutions

To conclude, the dynamic viscosity of the HPAM solution can be maintained at low levels of monovalent salts. The presence of 1,000 ppm divalent salts can lead significant drop in dynamic viscosity. Iron ions in the aqueous solution can cause both reducing in viscosity and stability. The precipitation of HPAM molecules appears in the slickwater despite the concentration of iron ions as low as 1,000 ppm. When the iron ion concentration is higher than 10,000 ppm, HPAM powder has difficulty dissolving and hydrolyzing. Overall, either a high concentration of monovalent

cations or a low concentration of divalent cations can cause viscosity loss; the HAPM is incompatible when iron ions are present in the aqueous solution.

Chapter 9 Limitation, Future Work, and Conclusion

9.1 Limitation and Future Work

1. The brine we used in this study to conduct the EO water treatment process includes synthetic FB, NaCl, Na₂SO₄, and CaCl₂ solutions. Though synthetic FB has a complex ionic composition, it still cannot represent the condition of produced water after hydraulic fracturing operations, which also contains organic matter and possible fracturing additives. In the next step of our research, we will also treat produced fracturing water to study the effect of the EO process on oxidizing organic matter and additives in fracturing water. The change in ion composition and fluid properties of fracturing water before and after the water treatment will also be investigated.
2. We used brine with 90,000 and 45,000 ppm salinity to conduct experiments. However, more cases with different salinities should be used to investigate the effects of salinity on wettability and oil recovery performance after the EO treatment.
3. All experiments were carried out under ambient temperature and pressure. More experiments should be conducted under reservoir conditions.
4. In this study, we mainly focused on the effects of two products (H₂O₂, and ClO⁻) after the EO process on fluid properties and rock wettability. However, S₂O₈²⁻ can also be produced in the EO process if enough sulfate ions are present in the brine. Future studies should investigate the effects of produced S₂O₈²⁻ on the fluid properties and rock wettability.
5. The concentration of generated oxidants by the EO process strongly depends on the treatment time. The concentration of the oxidants will be higher if we treat the brine for a long time. Future studies should increase the dose of oxidants in the contact-angle and spontaneous imbibition experiments to investigate its effects on the results.

6. We observed reddish-brown precipitates on the rock surface when the rock samples were soaked in treated water or untreated water + NaOCl. The precipitates are likely $\text{Fe}(\text{OH})_3$, produced by the reaction between pyrite (FeS_2) and OCl^- . However, a further analysis is required to confirm the composition of the precipitates.
7. Before and after spontaneous imbibition, the brine composition should be further analyzed to investigate the possible reactions between the rock and the soaking fluid.
8. In this study, we only conducted spontaneous countercurrent imbibition experiments to test the efficiency of brine treated by the EO process in enhancing oil recovery. The purpose of countercurrent imbibition is to see if the EO process can generally give more oil recovery by changing the rock wettability. Thus, our experiments do not consider the other parameters that may influence the oil recovery, such as pore size, permeability, and pore connectivity. Our experimental results did not give definitive proof of oil recovery enhancement. Core flooding tests should be conducted to investigate the effects of these parameters during waterflooding processes using treated and untreated water samples.
9. The threshold concentration for the problematic ions that incompatible with HPAM should be more accurate, therefore more salinity should be investigated. Also, viscoelastic properties should be conducted for evaluating the ability on proppant transportation.
10. Friction flow loop tests and particle settling tests should be conducted to evaluate the drag reduction and terminal velocity.
11. The results of sensitivity tests for problematic ions can be applied to design a cost-effective procedure for treating produced water while maintaining the stability of friction reducers. In the future, we will design a treatment procedure to treat the produced water using a combination of

oxidation, lime softening, and nanofiltration techniques to reduce the concentration of the problematic ions. Then we will use the treated brine to conduct dynamic viscosity, particles size distribution, viscoelasticity measurements, friction flow loop test and settling test to check the possibility of reusing produced water for hydraulic fracturing.

9.2 Conclusion

The objectives of this study were to 1) investigate the effects of water treatment by the EO process on rock wettability and imbibition oil recovery 2) determine if the produced FB can be used for fracturing fluid preparation and identify the problematic ions for removal. To achieve those objectives, we conducted:

1) systematic CA and spontaneous imbibition experiments using rock and oil samples from the Montney Formation and various aqueous solutions to evaluate the change in water composition and rock wettability by the EO process.

2) dynamic viscosity, particle size distribution, and viscoelastic properties measurements with HPAM in different aqueous solution, including DI water, FB, NaCl, CaCl₂, MgCl₂, FeSO₄ solutions with various salinity, to evaluate the possibility of reuse produced brine for fracturing fluid preparation

The key findings are summarized here:

1. The CA values of oil droplets on the rock surface soaked in the treated synthetic formation brine (90,000 and 45,000 ppm), NaCl (90,000 and 45,000 ppm), and Na₂SO₄ solutions are $84.9^\circ \pm 2.8^\circ$, $89.6^\circ \pm 3.9^\circ$, $73.3^\circ \pm 7.3^\circ$, $73.8^\circ \pm 9.4^\circ$, and $69.9^\circ \pm 2.8^\circ$, respectively, which are higher than those in untreated brine ($71.8^\circ \pm 4.6^\circ$, $75.0^\circ \pm 5.1^\circ$, $65.9^\circ \pm 7.1^\circ$, $60.3^\circ \pm 4.5^\circ$, and $60.9^\circ \pm 2.9^\circ$, respectively), indicating that the rock is less

oil-wet in treated brine, NaCl, and Na₂SO₄ solutions. The CA of oil droplets on the rock surface in the treated CaCl₂ solution ($46.6^\circ \pm 7.4^\circ$) is lower than that in the untreated one ($60.5^\circ \pm 4.7^\circ$), indicating that the rock is more oil-wet in the treated CaCl₂ solution. The results can be explained by strong Ca²⁺ bridging between the rock and the oil, providing additional attraction between the rock and the oil in CaCl₂ solutions.

2. The oil CA increases from 73 to 87° by increasing the pH value of the NaCl solution, changing the rock wettability toward less oil-wet conditions. A possible explanation is that rock and oil surfaces become more negatively charged with increasing pH. The stronger electrostatic repulsion between the rock and oil results in a less oil-wet condition. However, no significant change in oil CA is observed upon increasing or decreasing the pH of CaCl₂ solutions, possibly due to the formation of strong Ca²⁺ bridging between rock and oil, eliminating the effect of pH.

3. The diffusion of H₂O₂ toward oil droplets increases the oil CA from 68 to 76° in NaCl solution, but it does not change the oil CA in CaCl₂ solution. The rock becomes more water-wet in NaCl solution by adding H₂O₂, possibly due to organic matter dissolution. In CaCl₂ solution, the wettability cannot be altered because the Ca²⁺ bridge (which provides rock–oil attraction) balances the oxidation effect of H₂O₂.

4. The diffusion of sodium hypochlorite decreases the oil CA in both NaCl and CaCl₂ solutions since a substantial amount of high-valence cations is released from the alkali–mineral interaction. High-valence cations lead to a stronger bridging between the rock and oil compared with low-valence cations. The strong bridging between rock and oil results in a more oil-wet condition.

5. The spontaneous imbibition results indicate that improvement in oil production using the EO-treated brine is not guaranteed. The half plugs of core 1 and core 4 are soaked in the treated and untreated NaCl solutions, but the oil recovery results are contradictory. The half plug of core 1 soaked in untreated brine produces 19.3% of oil, while the other half in treated brine produces 22.7% of oil, indicating that use of treated brine in the EO process can slightly increase the oil production. However, the half plug of core 4 soaked in untreated brine produces 22.2% of oil, while the other half in treated brine produces 17.2% of oil. We observed significant reddish-brown precipitates on the surface of core 4, which can be the reason for the low recovery when using treated brine. The reddish-brown precipitates are also observed in untreated brine with NaOCl, indicating that they may be the product of active chlorine reactions with the rock minerals. The observed precipitates may block the pores near the rock surface, reducing oil production rate.

6. HPAM in the FB has a much lower viscosity profile along all the shear rate ranges compared to the HPAM in DI water. The hydrodynamic size of HPAM in the FB is smaller than the hydrodynamic size of HAPM in DI water. Viscoelastic properties results show that HPAM solution made with FB has higher storage modulus than loss modulus in the entire measured range, indicating a considerable curling of HPAM in the FB.

7. HPAM can resist low levels of monovalent salts. As the concentration of monovalent salts increases, the dynamic viscosity profile gradually shifts downward. Divalent ion concentrations as low as 1,000 ppm can dramatically reduce the dynamic viscosity. 100 ppm of Iron ions in the aqueous solution can cause both reducing in viscosity and stability. The precipitation of HPAM molecules appears in the slickwater despite the concentration

of iron ions as low as 1,000 ppm. When the iron ion concentration is higher than 10,000 ppm, HPAM powder has difficulty dissolving and hydrolyzing.

Chapter 10 Reference

Afekare, D., Garno, J., & Rao, D. (2021). Enhancing oil recovery using silica nanoparticles: Nanoscale wettability alteration effects and implications for shale oil recovery. *Journal of Petroleum Science & Engineering*, 203(108897), 108897. <https://doi.org/10.1016/j.petrol.2021.108897>

Al-Ghouti, M. A., Al-Kaabi, M. A., Ashfaq, M. Y., & Da'na, D. A. (2019). Produced water characteristics, treatment and reuse: A review. *Journal of Water Process Engineering*, 28, 222–239. <https://doi.org/10.1016/j.jwpe.2019.02.001>

Al-Hadhrami, H. S., & Blunt, M. J. (2001). Thermally induced wettability alteration to improve oil recovery in fractured reservoirs. *SPE Reservoir Evaluation & Engineering*, 4(03), 179–186. <https://doi.org/10.2118/71866-pa>

Al-Hajri, S., Negash, B. M., Rahman, M. M., Haroun, M., & Al-Shami, T. M. (2022). Perspective Review of Polymers as Additives in Water-Based Fracturing Fluids. *ACS omega*, 7(9), 7431-7443.

Alhammadi, A. M., AlRatrouf, A., Singh, K., Bijeljic, B., & Blunt, M. J. (2017). In situ characterization of mixed-wettability in a reservoir rock at subsurface conditions. *Scientific Reports*, 7(1), 10753. <https://doi.org/10.1038/s41598-017-10992-w>

Alias, N. H., Jaafar, J., Samitsu, S., Yusof, N., Othman, M. H. D., Rahman, M. A., Ismail, A. F., Aziz, F., Salleh, W. N. W., & Othman, N. H. (2018). Photocatalytic degradation of oilfield produced water using graphitic carbon nitride embedded in electrospun polyacrylonitrile nanofibers. *Chemosphere*, 204, 79–86. <https://doi.org/10.1016/j.chemosphere.2018.04.033>

Arthur, J. D., Langhus, B. G., & Patel, C. (2005). *Technical Summary of Oil & Gas Produced Water Treatment Technologies*. All Consulting.

Arthur, J. Daniel, Bohm, B., & Cornue, D. (2009). *Environmental considerations of modern shale gas development*. All Days.

Ba Geri, M., Ellafi, A., Flori, R., Noles, J., & Kim, S. (2019). Viscoelastic characterization effect of high-viscosity friction reducers and proppant transport performance in high-TDS environment. Day 1 Mon, September 30, 2019.

Ba Geri, M., Imqam, A., Bogdan, A., & Shen, L. (2019). Investigate the rheological behavior of high viscosity friction reducer fracture fluid and its impact on proppant static settling velocity. Day 2 Wed, April 10, 2019.

Bai, J.-M., Fan, W.-Y., Nan, G.-Z., Li, S.-P., & Yu, B.-S. (2010). Influence of Interaction between Heavy Oil Components and Petroleum Sulfonate on the Oil–Water Interfacial Tension. *J. Dispers. Sci. Technol*, 551–556.

Bhagawan, D., Poodari, S., Golla, S., Himabindu, V., & Vidyavathi, S. (2016). Treatment of the petroleum refinery wastewater using combined electrochemical methods. *Desalination and Water Treatment*, 57(8), 3387–3394. <https://doi.org/10.1080/19443994.2014.987175>

Biheri, G., & Imqam, A. (2021a). Experimental Study: High Viscosity Friction Reducer Fracture Fluid Rheological Advantages Over the Guar Linear Gel. In *55th US Rock Mechanics/Geomechanics Symposium*.

Biheri, G., & Imqam, A. (2021b). Settling of Spherical Particles in High Viscosity Friction Reducer Fracture Fluids. *Energies*, 14(9).

Boczka, G., & Fernandes, A. (2017). Wastewater treatment by means of advanced oxidation processes at basic pH conditions: A review. *Chemical Engineering Journal (Lausanne, Switzerland: 1996)*, 320, 608–633. <https://doi.org/10.1016/j.cej.2017.03.084>

Brady, P. V., & Krumhansl, J. L. (2012). A Surface Complexation Model of Oil-Brine-Sandstone Interfaces at 100 C: Low Salinity Waterflooding. *J. Pet. Sci. Eng*, 81, 171–176.

Brady, Patrick V., Krumhansl, J. L., & Mariner, P. E. (2012). Surface complexation modeling for improved oil recovery. *All Days*.

Cañizares, P., Sáez, C., Lobato, J., & Rodrigo, M. A. (1944). Electrochemical Treatment of 4-Nitrophenol-Containing Aqueous Wastes Using Boron-Doped Diamond Anodes. *Ind. Eng. Chem. Res*, 43.

Chen, Q., You, L., Kang, Y., Dou, L., & Sheng, J. J. (2018). Gypsum Crystallization-Induced Fracturing during Shale–Fluid Reactions and Application for Shale Stimulation. *Energy Fuels*, 32, 10367–10381.

Chen, Qiang, Kang, Y., You, L., Yang, P., Zhang, X., & Cheng, Q. (2017). Change in composition and pore structure of Longmaxi black shale during oxidative dissolution. *International Journal of Coal Geology*, 172, 95–111. <https://doi.org/10.1016/j.coal.2017.01.011>

Cheng, Q., You, L., Kang, Y., Zhou, Y., & Zhang, N. (2021). Oxidative dissolution kinetics of organic-rich shale by hydrogen peroxide (H₂O₂) and its positive effects on improving fracture conductivity. *Journal of Natural Gas Science and Engineering*, 89(103875), 103875. <https://doi.org/10.1016/j.jngse.2021.103875>

Chu, Y. Y., Qian, Y., Wang, W. J., & Deng, X. L. (2012). A dual-cathode electro-Fenton oxidation coupled with anodic oxidation system used for 4-nitrophenol degradation. *Journal of Hazardous Materials*, 199–200, 179–185. <https://doi.org/10.1016/j.jhazmat.2011.10.079>

De Ruiter, R. (2005). Manipulation of Drops with Electrowetting. *Condens. Matter*, 17, R705–R774.

Dong, W., & Wan, J. (2014). Additive Surface Complexation Modeling of Uranium (VI) Adsorption onto Quartz-Sand Dominated Sediments. *Environ. Sci. Technol*, 48, 6569–6577.

Eia, U. (2016). Trends in US Oil and Natural Gas Upstream Costs. US Energy Information Administration.

Ely, J. W., Horn, A., Cathey, R., Fraim, M., & Jakhete, S. (2011). Game changing technology for treating and recycling frac water. *All Days*.

Escudier, P., & Smith, S. (2001). Fully developed turbulent flow of non-Newtonian liquids through a square duct. *Proceedings. Mathematical, Physical, and Engineering Sciences*, 457(2008), 911–936. <https://doi.org/10.1098/rspa.2000.0698>

Evangelou, V. P. (bill), & Zhang, Y. L. (1995). A review: Pyrite oxidation mechanisms and acid mine drainage prevention. *Critical Reviews in Environmental Science and Technology*, 25(2), 141–199. <https://doi.org/10.1080/10643389509388477>

Fakhru'l-Razi, A., Pendashteh, A., Abdullah, L. C., Biak, D. R. A., Madaeni, S. S., & Abidin, Z. Z. (2009). Review of technologies for oil and gas produced water treatment. *Journal of Hazardous Materials*, 170(2–3), 530–551. <https://doi.org/10.1016/j.jhazmat.2009.05.044>

Feng, X., Simpson, A. J., & Simpson, M. J. (2005). Chemical and mineralogical controls on humic acid sorption to clay mineral surfaces. *Organic Geochemistry*, 36(11), 1553–1566. <https://doi.org/10.1016/j.orggeochem.2005.06.008>

Fernø, M. A., Torsvik, M., Haugland, S., Graue, A., Graue, A., Aspenes, E., Bognø, T., Moe, R. W., & Ramsdal, J. (2002). Alteration of Wettability and Wettability Heterogeneity. *J. Pet. Sci. Eng*, 24(57), 3–17.

Fjelde, I., Omekeh, A. V., & Haugen, P. E. (2017). Effect of Ferrous Ion Fe²⁺ on Wettability: Oxidation and Cation Bridging. In Day 3 Wed. SPE.

Fraim, M., & Jakhete, S. (2015). Sustainable flow back and produced water treatment using A next generation ElectroOxidation reactor. Day 2 Tue, September 29, 2015.

Ganiyu, S. O., & Gamal El-Din, M. (n.d.). Insight into In-Situ Radical and Non-Radical Oxidative Degradation of Organic Compounds in Complex Real Matrix during Electro-Oxidation with Boron Doped Diamond Electrode: A Case Study of Oil Sands Process Water Treatment. *Appl. Catal*, 2020.

Ganiyu, S. O., & Martínez-Huitle, C. A. (2019). Mechanisms and Reactivity of Electrogenerated Reactive Species at Thin-film Borondoped Diamond (BDD) Electrodes during Electrochemical Wastewater Treatment. *ChemElectroChem*, 6, 2379–2392.

Gargouri, B., Gargouri, O. D., Gargouri, B., Trabelsi, S. K., Abdelhedi, R., & Bouaziz, M. (2014). Application of electrochemical technology for removing petroleum hydrocarbons from produced water using lead dioxide and boron-doped diamond electrodes. *Chemosphere*, 117, 309–315. <https://doi.org/10.1016/j.chemosphere.2014.07.067>

Gbadamosi, A. O., Junin, R., Manan, M. A., Yekeen, N., & Augustine, A. (2019). Hybrid suspension of polymer and nanoparticles for enhanced oil recovery. *Polymer Bulletin (Berlin, Germany)*, 76(12), 6193–6230. <https://doi.org/10.1007/s00289-019-02713-2>

Government Of Canada CER Canada Energy Regulator/Regie de l'energie Du Canada; 2021.

Graue, A., Aspenes, E., Bognø, T., Moe, R. W., & Ramsdal, J. (2002). Alteration of wettability and wettability heterogeneity. *Journal of Petroleum Science & Engineering*, 33(1–3), 3–17. [https://doi.org/10.1016/s0920-4105\(01\)00171-1](https://doi.org/10.1016/s0920-4105(01)00171-1)

Gu, X., & Evans, L. J. (2007). Pb (II), and Zn (II) onto Fithian Illite. Ni (II), 307, 317–325.

Guo, Y., Zhang, M., Yang, H., Wang, D., Ramos, M. A., Hu, T. S., & Xu, Q. (2022). Friction challenge in hydraulic fracturing. *Lubricants* (Basel, Switzerland), 10(2), 14. <https://doi.org/10.3390/lubricants10020014>

Habibi, A., Dehghanpour, H., Binazadeh, M., Bryan, D., & Uswak, G. (2016). Advances in understanding wettability of tight oil formations: A Montney case study. *SPE Reservoir Evaluation & Engineering*, 19(04), 583–603. <https://doi.org/10.2118/175157-pa>

Hand, S., & Cusick, R. D. (2021). Electrochemical disinfection in water and wastewater treatment: Identifying impacts of water quality and operating conditions on performance. *Environmental Science & Technology*, 55(6), 3470–3482. <https://doi.org/10.1021/acs.est.0c06254>

Haugen, P. E. (2016). Characterization of wettability alteration by flotation.

Hu, S., Hu, J., Sun, Y., Zhu, Q., Wu, L., Liu, B., Xiao, K., Liang, S., Yang, J., & Hou, H. (2021). Simultaneous Heavy Metal Removal and Sludge Deep Dewatering with Fe (II) Assisted Electro-Oxidation Technology. *J. Hazard. Mater.*, 405.

Hu, Y., Chu, Z., Dai, C., Wang, F., Ren, H., Jin, X., & Wu, Y. (2021). Probing of the hydrated cation bridges in the oil/brine/silica system via atomic force microscopy and molecular dynamics simulation. *Fuel* (London, England), 306(121666), 121666. <https://doi.org/10.1016/j.fuel.2021.121666>

Ibrahim, D. S., Devi, P. S., & Balasubramanian, N. (2013). Electrochemical Oxidation Treatment of Petroleum Refinery Effluent. *Int. J. Sci. Eng. Res*, 8, 1–5.

Igunnu, E. T., & Chen, G. Z. (2014).) Eia, U. Trends in US Oil and Natural Gas Upstream Costs. *Int. J. Low-Carbon Technol*, 9(6), 157–177.

Igunnu, Ebenezer T., & Chen, G. Z. (2014). Produced water treatment technologies. *International Journal of Low-Carbon Technologies*, 9(3), 157–177. <https://doi.org/10.1093/ijlct/cts049>

Israelachvili, J. N. (2011). *Intermolecular and Surface Forces*; 905 Academic Press (Vol. 905). Academic Press.

Jew, A. D., Dustin, M. K., Harrison, A. L., Joe-Wong, C. M., Thomas, D. L., Maher, K., Brown, G. E., Jr, & Bargar, J. R. (2017). Impact of organics and carbonates on the oxidation and precipitation of iron during hydraulic fracturing of shale. *Energy & Fuels: An American Chemical Society Journal*, 31(4), 3643–3658. <https://doi.org/10.1021/acs.energyfuels.6b03220>

Kathel, P., & Mohanty, K. K. (2013). Wettability alteration in a tight oil reservoir. *Energy & Fuels: An American Chemical Society Journal*, 27(11), 6460–6468. <https://doi.org/10.1021/ef4012752>

Keleşođlu, S., Meakin, P., & Sjöblom, J. (2011). Effect of Aqueous Phase PH on the Dynamic Interfacial Tension of Acidic Crude Oils and Myristic Acid in Dodecane. *J. Dispers. Sci. Technol*, 32, 1682–1691.

Kobayashi, K., Liang, Y., Murata, S., Matsuoka, T., Takahashi, S., Amano, K.-I., Nishi, N., & Sakka, T. (2017). Stability Evaluation of Cation Bridging on Muscovite Surface for Improved Description of IonSpecific Wettability Alteration. *J. Phys. Chem. C*, 9273–9281.

Kuila, U., McCarty, D. K., Derkowski, A., Fischer, T. B., Topór, T., & Prasad, M. (2014). Nano-scale texture and porosity of organic matter and clay minerals in organic-rich mudrocks. *Fuel* (London, England), 135, 359–373. <https://doi.org/10.1016/j.fuel.2014.06.036>

Kumar, N., & Mandal, A. (n.d.). Wettability Alteration of Sandstone Rock by Surfactant Stabilized Nanoemulsion for Enhanced Oil Recovery 焘 A Mechanistic Study. *Colloids Surf. A Physicochem. Eng. Asp*, 2020.

Kunhi Mouvenchery, Y., Kučerík, J., Diehl, D., & Schaumann, G. E. (2012). Cation-mediated cross-linking in natural organic matter: a review. *Re/Views in Environmental Science and Bio/Technology*, 11(1), 41–54. <https://doi.org/10.1007/s11157-011-9258-3>

Lawal, T., Wang, M., Abeykoon, G. A., Argüelles-Vivas, F. J., & Okuno, R. (2022). Effect of chemical partition behavior on oil recovery by wettability alteration in fractured tight reservoirs. *Energy & Fuels: An American Chemical Society Journal*, 36(2), 797–805. <https://doi.org/10.1021/acs.energyfuels.1c03344>

Len, S.-V., Hung, Y.-C., Chung, D., Anderson, J. L., Erickson, M. C., & Morita, K. (2002). Effects of storage conditions and pH on chlorine loss in electrolyzed oxidizing (EO) water. *Journal of Agricultural and Food Chemistry*, 50(1), 209–212. <https://doi.org/10.1021/jf010822v>

Li, Y., Yang, S., Liu, D., Yang, C., Yang, Z., Li, H., & Tang, Z. (2020). Experimental study of shale-fluids interaction during oxidative dissolution with hydrogen peroxide, sodium hypochlorite and sodium persulfate. *Applied Geochemistry: Journal of the International Association of Geochemistry and Cosmochemistry*, 113(104503), 104503. <https://doi.org/10.1016/j.apgeochem.2019.104503>

Liang, X., & Sheng, J. J. (2020). Comparison of Chemical-Induced Fracturing by Na₂S₂O₈, NaClO, and H₂O₂ in Marcellus Shale. *Energy Fuels*, 34, 15905–15919.

Liu, Fang-Jing, Wei, X.-Y., Zhu, Y., Wang, Y.-G., Li, P., Fan, X., Zhao, Y.-P., Zong, Z.-M., Zhao, W., & Wei, Y.-B. (2013). Oxidation of Shengli lignite with aqueous sodium hypochlorite promoted by pretreatment with aqueous hydrogen peroxide. *Fuel (London, England)*, 111, 211–215. <https://doi.org/10.1016/j.fuel.2013.04.041>

Liu, F.-J., Wei, X.-Y., Zhu, Y., Gui, J., Wang, Y.-G., Fan, X., Zhao, Y.-P., & Zong, Z.-M. (2013). Investigation on Structural Features of Shengli Lignite through Oxidation under Mild Conditions. *Fuel*, 109, 316–324.

Malhotra, S., & Sharma, M. M. (2012). Settling of spherical particles in unbounded and confined surfactant-based shear thinning viscoelastic fluids: An experimental study. *Chemical Engineering Science*, 84, 646–655. <https://doi.org/10.1016/j.ces.2012.09.010>

Mccurdy, R. (n.d.). Underground Injection Wells for Produced Water Disposal. In *Proceedings of the Technical Workshops for the Hydraulic Fracturing Study: Water Resources*.

Medir, M., & Giralt, F. (1982). Stability of chlorine dioxide in aqueous solution. *Water Research*, 16(9), 1379–1382. [https://doi.org/10.1016/0043-1354\(82\)90221-4](https://doi.org/10.1016/0043-1354(82)90221-4)

Muller, G., Laine, J. P., & Fenyo, J. C. (1979). High-molecular-weight hydrolyzed polyacrylamides. I. Characterization. Effect of salts on the conformational properties. *Journal of Polymer Science Polymer Chemistry Edition*, 17(3), 659–672. <https://doi.org/10.1002/pol.1979.170170305>

Paktinat, J., O'Neil, B., Aften, C., & Hurd, M. (2011a). Critical evaluation of high brine tolerant additives used in shale slick water fracs. *All Days*.

Paktinat, J., O'Neil, B., Aften, C., & Hurd, M. (2011b). High brine tolerant polymer improves the performance of slickwater frac in shale reservoirs. *All Days*.

Peters, R. A. (1931). Interfacial tension and hydrogen-ion concentration. *Proceedings of the Royal Society of London. Series B, Containing Papers of a Biological Character*. Royal Society (Great Britain), 109(760), 88–90. <https://doi.org/10.1098/rspb.1931.0070>

Petkov, L. (2009). Electrooxidation of Chloride Systems. A Review. *Oxid. Commun*, 32, 654–677.

Pu, W., Shen, C., Pang, S., Tang, X., Tian, Q., & Song, Y. (2018). Properties of emulsions formed in situ in a heavy-oil reservoir during water flooding: Effects of salinity and pH. *Journal of Surfactants and Detergents*, 21(5), 699–710. <https://doi.org/10.1002/jsde.12188>

Pulkka, S., Martikainen, M., Bhatnagar, A., & Sillanpää, M. (2014). Electrochemical Methods for the Removal of Anionic Contaminants from Water—a Review. *Sep. Purif. Technol*, 132(2).

Regulator, A. E. (2019). ST98: Alberta Energy Outlook. Alberta Energy Regulator.

Rezazadeh, M., Khajeh, A., & Mesbah, M. (2018). Membrane filtration of wastewater from gas and oil production. *Environmental Chemistry Letters*, 16(2), 367–388. <https://doi.org/10.1007/s10311-017-0693-4>

Rocha, J. H. B., Gomes, M. M. S., Fernandes, N. S., da Silva, D. R., & Martínez-Huitle, C. A. (2012). Application of electrochemical oxidation as alternative treatment of produced water generated by Brazilian petrochemical industry. *Fuel Processing Technology*, 96, 80–87. <https://doi.org/10.1016/j.fuproc.2011.12.011>

Rostami, P., Mehraban, M. F., Sharifi, M., Dejam, M., & Ayatollahi, S. (2019). Effect of water salinity on oil/brine interfacial behaviour during low salinity waterflooding: A mechanistic study. *Petroleum*, 5(4), 367–374. <https://doi.org/10.1016/j.petlm.2019.03.005>

Ryan, D. R., Maher, E. K., Heffron, J., Mayer, B. K., & McNamara, P. J. (2021). Electrocoagulation-electrooxidation for mitigating trace organic compounds in model drinking water sources. *Chemosphere*, 273(129377), 129377. <https://doi.org/10.1016/j.chemosphere.2020.129377>

Sanaei, A., Tavassoli, S., & Sepehrnoori, K. (2019). Investigation of modified Water chemistry for improved oil recovery: Application of DLVO theory and surface complexation model. *Colloids and Surfaces. A, Physicochemical and Engineering Aspects*, 574, 131–145. <https://doi.org/10.1016/j.colsurfa.2019.04.075>

Santos, E. V., Sena, E. V., Da Silva, D. R., Ferro, D. R., De Battisti, A., & Martínez-Huitle, A. (2014). Scale-up of Electrochemical Oxidation System for Treatment of Produced Water Generated by Brazilian Petrochemical Industry. *Environ. Sci. Pollut. Res*, 21.

Shih, J.-S., Saiers, J. E., Anisfeld, S. C., Chu, Z., Muehlenbachs, L. A., & Olmstead, S. M. (2015). Characterization and analysis of liquid waste from Marcellus Shale gas development. *Environmental Science & Technology*, 49(16), 9557–9565. <https://doi.org/10.1021/acs.est.5b01780>

Silva, I. P., Aguiar, A. A., Rezende, V. P., Monsores, A. L., & Lucas, E. F. (2018). A polymer flooding mechanism for mature oil fields: Laboratory measurements and field results interpretation. *Journal of Petroleum Science and Engineering*, 161, 468–475.

Silveira, B. M. de O., Gioria, R. dos S., Florez, J. J. A., Fagundes, T. B., Silva, M. A. da T., Skinner, R., Ulsen, C., Carneiro, C. de C., & Ferrari, J. V. (2022). Influence of oil aging time, pressure and temperature on contact angle measurements of reservoir mineral surfaces. *Fuel* (London, England), 310(122414), 122414. <https://doi.org/10.1016/j.fuel.2021.122414>

Sun, H., Wood, B., Stevens, D., Cutler, J., Qu, Q., & Lu, M. (2011). A Nondamaging Friction Reducer for Slickwater Frac Applications. *All Days*.

Sun, H., Zhou, J., Cutler, J., Royce, T., Nelson, S., & Qu, Q. (2013). Field case histories of a non-damaging guar alternative for linear gel application in Slickwater fracturing. *All Days*.

Sun, Y., Wu, Q., Wei, M., Bai, B., & Ma, Y. (2014). Experimental study of friction reducer flows in microfracture. *Fuel* (London, England), 131, 28–35. <https://doi.org/10.1016/j.fuel.2014.04.050>

Tamamura, S., Ueno, A., Aramaki, N., Matsumoto, H., Uchida, K., Igarashi, T., & Kaneko, K. (2015). Effects of oxidative weathering on the composition of organic matter in coal and sedimentary rock. *Organic Geochemistry*, 81, 8–19. <https://doi.org/10.1016/j.orggeochem.2015.01.006>

Taylor, K. C., & Nasr-El-Din, H. A. (2007). Hydrophobically associating polymers for oil field applications. *Canadian International Petroleum Conference*.

Thomas, M. (2011). The effect of supplementary cementing materials on alkali-silica reaction: A review. *Cement and Concrete Research*, 41(12), 1224–1231. <https://doi.org/10.1016/j.cemconres.2010.11.003>

Tian, H., Liu, F., Jin, X., & Wang, M. (2019). Competitive effects of interfacial interactions on ion-tuned wettability by atomic simulations. *Journal of Colloid and Interface Science*, 540, 495–500. <https://doi.org/10.1016/j.jcis.2018.12.108>

Tian, H., & Wang, M. (2017). Electrokinetic mechanism of wettability alternation at oil-water-rock interface. *Surface Science Reports*, 72(6), 369–391. <https://doi.org/10.1016/j.surfrep.2018.01.001>

Tran, S., Yassin, M. R., Eghbali, S., Doranehgard, M. H., & Dehghanpour, H. (n.d.). Quantifying Oil-Recovery Mechanisms during Natural-Gas Huff 'n' Puff Experiments on Ultratight Core Plugs. *SPE J*, 26, 498–514.

Treviño-Reséndez, J. D. J., Medel, A., & Meas, Y. (2021). Electrochemical Technologies for Treating Petroleum Industry Wastewater. *Curr. Opin. Electrochem*, 27.

Tunega, D., Aquino, A. J. A., Haberhauer, G., Lischka, H., Schaumann, G. E., & Gerzabek, M. H. (2014). Molecular models of cation and water molecule bridges in humic substances. In *Soil Carbon* (pp. 107–115). Springer International Publishing.

Uhlig, H. H. (1937). The solubilities of gases and surface tension. *The Journal of Physical Chemistry*, 41(9), 1215–1226. <https://doi.org/10.1021/j150387a007>

Wang, L., Wang, D., Shen, Y., Lai, X., & Guo, X. (2016). Study on properties of hydrophobic associating polymer as drag reduction agent for fracturing fluid. *Journal of Polymer Research*, 23(11). <https://doi.org/10.1007/s10965-016-1129-8>

Wang, X., Zhou, M., Meng, X., Wang, L., & Huang, D. (2016). Effect of Protein on PVDF Ultrafiltration Membrane Fouling Behavior under Different PH Conditions: Interface Adhesion Force and XDLVO Theory Analysis. *Front. Environ. Sci. Eng*, 10.

Wang, Y., Lu, T., Zhang, H., Li, Y., Song, Y., Chen, J., Fu, X., Qi, Z., & Zhang, Q. (2020). Factors affecting the transport of petroleum colloids in saturated porous media. *Colloids and Surfaces. A, Physicochemical and Engineering Aspects*, 585(124134), 124134. <https://doi.org/10.1016/j.colsurfa.2019.124134>

Wang, Q., Mao, J., Zhao, J., Zhang, H., Xue, J., Zhang, Q., ... & Peng, R. (2022). Synthesis of a salt-responsive hydrophobically associating polymer for fracturing fluid based on self-assembling transition. *Journal of Molecular Liquids*, 120201.

Watanabe, H., & Iizuka, K. (1986). The influence of dissolved gases on the density of water. *Metrologia*, 22(2), 115–115. <https://doi.org/10.1088/0026-1394/22/2/007>

Wei, J., Jia, W., Zuo, L., Chen, H., & Feng, Y. (2022). Turbulent drag reduction with an ultra-high-molecular-weight water-soluble polymer in slick-water hydrofracking. *Molecules (Basel, Switzerland)*, 27(2), 351. <https://doi.org/10.3390/molecules27020351>

Wyatt, N. B., Gunther, C. M., & Liberatore, M. W. (2011). Drag reduction effectiveness of dilute and entangled xanthan in turbulent pipe flow. *Journal of Non-Newtonian Fluid Mechanics*, 166(1–2), 25–31. <https://doi.org/10.1016/j.jnnfm.2010.10.002>

Yang, B., Zhao, J., Mao, J., Tan, H., Zhang, Y., & Song, Z. (2019). Review of friction reducers used in slickwater fracturing fluids for shale gas reservoirs. *Journal of Natural Gas Science and Engineering*, 62, 302–313. <https://doi.org/10.1016/j.jngse.2018.12.016>

Yang, S., Liu, D., Li, Y., Yang, C., Yang, Z., Chen, X., Li, H., & Tang, Z. (2020). Experimental study on the oxidative dissolution of carbonate-rich shale and silicate-rich shale with H₂O₂, Na₂S₂O₈ and NaClO: Implication to the shale gas recovery with oxidation stimulation. *Journal of Natural Gas Science and Engineering*, 76(103207), 103207. <https://doi.org/10.1016/j.jngse.2020.103207>

Yap, N. T. (2016). Unconventional shale gas development: challenges for environmental policy and EA practice. *Impact Assessment and Project Appraisal*, 34(2), 97–109. <https://doi.org/10.1080/14615517.2016.1176405>

Yu, W., Lei, J., Wang, T., & Chen, W. (2019). H₂O₂-enhanced shale gas recovery under different thermal conditions. *Energies*, 12(11), 2127. <https://doi.org/10.3390/en12112127>

Yuan, L., Dehghanpour, H., & Ceccanese, A. (2019). Imbibition oil recovery from the Montney core plugs: The interplay of wettability, osmotic potential and microemulsion effects. Day 2 Wed, April 24, 2019.

Yuan, L., Zhang, Y., & Dehghanpour, H. (2021). A theoretical explanation for wettability alteration by adding nanoparticles in oil-water-tight rock systems. *Energy & Fuels: An American Chemical Society Journal*, 35(9), 7787–7798. <https://doi.org/10.1021/acs.energyfuels.1c00001>

Zeng, L., Chen, Y., Lu, Y., Lau, H. C., Hossain, M. M., Saeedi, A., & Xie, Q. (2019). Interpreting water uptake by shale with ion exchange, surface complexation, and disjoining pressure. *Energy & Fuels: An American Chemical Society Journal*, 33(9), 8250–8258. <https://doi.org/10.1021/acs.energyfuels.9b01732>

Zhao, H., Danican, S., Torres, H., Christanti, Y., Nikolaev, M., Makarychev-Mikhailov, S., & Bonnell, A. (2018). Viscous slickwater as enabler for improved hydraulic fracturing design in unconventional reservoirs. Day 2 Tue, September 25, 2018.

Zhou, Y., Lei, Y., Chen, W., & Yu, W. (2018). Enhance low temperature oxidization of shale gas recovery using hydrogen peroxide. *Journal of Petroleum Science & Engineering*, 164, 523–530. <https://doi.org/10.1016/j.petrol.2018.01.053>